UNIVERSITY OF CALIFORNIA,
IRVINE

Aging Immunity: Monocyte Derived Dendritic Cell's Metabolic Shift associated with Human Aging

THESIS

submitted in partial satisfaction of the requirements
for the degree of

MASTER OF SCIENCE

in Biomedical Engineering

by

Albert Liu

Thesis Committee:
Professor Abraham Lee, Chair
Associate Professor Anshu Agrawal
Assistant Professor Michelle Digman

2018

DEDICATION

To

My grandfather.

TABLE OF CONTENTS

LIST OF FIGURES

LIST OF TABLES

ACKNOWLEDGMENTS

I would first like to acknowledge my family for their unconditional love and support. I am grateful for all the sacrifices they have made so I can pursue my dreams. I would not be here today without their continual guidance and inspiration.

This thesis would not have been possible without the aid and support of my lab mates. I sincerely thank Xuan Li for training and helping me throughout my different experiments. I am especially appreciative of her giving up hours of her time to teach and assist me in the design and fabrication of the microfluidic devices. I thank also to Mohammad Aghaamoo for aiding me in performing FEM simulations. The thesis would not be as awesome otherwise without simulation modeling. I would also like to express my gratitude to Neha Garg, Da Zhao and Dr. Tao Yue for providing me with advices and assistance throughout my degree. Their support was incredibly helpful and encouraging. I want to extend special thanks to Silin Cai for being an excellent undergraduate research assistance. His assistant on miscellaneous tasks, image processing, and data analysis was what made the completion of this thesis possible.

For my advisors, I would like to thank my thesis committee chair and advisor, Professor Abraham P. Lee for allowing me to join his lab. Without him, this project would never have been started and I am grateful for the guidance and support he gave along the way. I would like to also extend my gratitude towards Professor Anshu Agrawal and Sudhandshu Agrawal for providing me with the samples and brilliant insights in the results. From them, I learned an incredible amount of knowledge whether it be from immunology, wet lab, or statistical analysis. They provided me an invaluable experience and made my degree worthwhile. Lastly, I would like to thank Professor Michelle Digman and her lab in assisting me in performing my imaging. She has given me the amazing opportunity to work with state of the art imaging technology. Special thanks to Dr. Rachel Cinco-Hedde and Ning Ma for training and assisting me in the operation of laser scanning microscope and the accompanying software.

Financial support of this project was made possible by University of California, Irvine, NSF I/UCRC Grant 1738617: CADMIM, and NIH/NIA-Award No. AG045216. Permission to reproduce figure from Cinco *et al.*'s work from *Biology of Reproduction* was given by Oxford University Press (LN: 4360620111637).

ABSTRACT OF THE THESIS

Aging Immunity: Monocyte Derived Dendritic Cell's Metabolic Shift associated with Human Aging

By

Albert Liu

Master of Science in Biomedical Engineering

University of California, Irvine, 2018

Professor Abraham P. Lee, Chair

Human aging is often linked to the gradual decline of the immune system. This age-related decline of the immune system, or immunosenescence, is often attributed to the increased frequency of elder morbidity and mortality. One prominent immunosenescence feature is that of a low grade chronic inflammation. Dendritic cells (DC) play a major role in inducing adaptive immunity by presenting pathogenic antigens at T-Cells to initiate immune response. Once activated, dendritic cells undergo physiological transformation and express a host of costimulatory and pro-inflammatory molecules. This transformation requires a shift in metabolic demand to meet the bioenergetic and biosynthetic needs of activated dendritic cells. We hypothesized that aging initiates excessive dendritic cell activation which could in turn triggers chronic inflammation observed in elderly subjects. As such, through studying known cellular metabolic markers from microfluidic aided fluorescence lifetime Imaging microscopy (FLIM) and flow cytometry, we report the preliminary results on the metabolic effects of aging on dendritic cells.

CHAPTER 1: INTRODUCTION

1.1 Problem Statement

Human aging is a universal multifarious process that increases the risk of frailty, disease susceptibility, and morbidity across different cell types, tissues, and organs[1]. While the causes of aging are unclear, encompassing factors from genetics, environmental, and stochastic events overtime could all contribute to the cause[1,2]. Age related diseases includes neurodegeneration, diabetes, atherosclerosis, osteoporosis, and metabolic syndrome to name a few[3]. Consequently, in conjunction with the ever increasing global life expectancy, there are strong interests in understanding the mechanisms of aging[4]. One key characteristic in aging is that of the general decline in the immune response. Often, elderly subjects display a chronic, systemic, low grade inflammation termed as "Inflammaging." Inflammaging is marked by a progressive increase in pro-inflammatory antigenic load and stress on cells[5,6]. This persistence of inflammatory stimuli is argued to cause diseases susceptibility as well as initiating inflammatory pathogenesis and tissue degeneration[7]. The etiology of this low-grade inflammation with age is not well understood but one theory suggests that damaged non-immune cells and protein aggregation accumulating with age lead can to pro-inflammatory cytokines that amplify the inflammatory response. The ambiguity and mystery of aging's effects on immune system has thus lead to considerable interests in revealing the mechanisms behind age related inflammatory response. Through controlling these mechanisms, novel immunotherapy to monitor and regulate immune response to combat deleterious effects of aging could be possible. Thus, we look forward to research and breakthrough in these areas for treatments in aging.

1.2 Proposed Solution

Within immune response, dendritic cells (DC) play a crucial role in the activation of adaptive immunity and regulation of inflammation. DCs are antigen presenting cells (APC) that present pathogenic antigens to T-cells. DCs accomplish this by constantly surveilling their surroundings for pathogens using pattern recognition receptors. Once DCs recognize a pathogen, they transform into an activated state to phagocytose the pathogens and present their antigens to T-cells. As such, aberrant behaviors of dendritic cells could lead to a myriad of immunogenic disorders[8]. Understanding the roles and mechanisms dendritic cells play in affecting age related immunological response would thus be a logical approach. Previous studies have observed alteration in signaling pathways in elderly subjects' dendritic cells. Mainly aged DCs display an increased activation of p38 MAP-kinase as well as increased activity of NF-κB p65. These signaling pathway alterations increase secretion of pro-inflammatory cytokines as well as the activation of dendritic cells[9,10]

The activation of DCs is marked by increased expression levels of costimulatory molecules and changes on surface MHC-peptide complexes[11]. These stimulatory molecules include the upregulation of a chemotactic receptor, CCR7, that induces dendritic cells to travel towards the lymph node where T-cells and B-Cells reside[12]. As such, the metabolic requirements to meet the bioenergetics and biosynthetic needs of a activated DC must be different to that of a quiescent DC with fewer anabolic demands[11]. Insight into the metabolic changes of activated dendritic cells could thus elucidate the mechanism of successful dendritic cell activation.

Therefore, it is possible to use metabolic states in dendritic cell to observe and control DC activation for immunotherapy applications.

One key metabolic characteristic of activated dendritic cells is that of metabolic pathway shift to glycolysis. This effect has been documented when dendritic cells are exposed to Toll Like Receptor (TLR) agonists such as lipopolysaccharide (LPS) in mice models[13,14]. The shift towards glycolysis is speculated to produce enough citrate in order to synthesize fatty acid, which is used for the enlargement of endoplasmic reticulum and Golgi apparatus during dendritic cell activation[15]. Thus, this shift in metabolic pathway could be used as an indicator for dendritic cell activation and as a method to monitor immune response.

Recent advances in fluorescence lifetime imaging microscopy (FLIM) have developed label-free methodologies to observe the intrinsic fluorescence markers of the cell. These fluorescence signals come from endogenous proteins and metabolites. One such fluorescent metabolic enzyme is the reduced form nicotinamide adenine dinucleotide (NADH)[16,17]. NADH is one of the main coenzymes involved in oxygen phosphorylation (OXPHOS) and glycolysis. In glycolysis, free NADH is produced thus raising the ratio of free NADH over enzyme bound NADH[18]. In OXPHOS, free NADH is oxidized into NAD^+, thus lowering the ratio of free NADH over bound NADH. As such, observing the unique fluorescence lifetime of free versus bound form of NADH, one could determine the dominant metabolic pathway employed by the cell. However, while FLIM is a powerful technique, microfluidics can substantially increase its effectiveness.

Microfluidics is a field specialized in manipulating small volumes of liquid. For cellular imaging, microfluidics is an excellent tool in handling cells due to its micron sized channels that match the size realm of cells. Thus, many different techniques and methodologies have been published to manipulate and trap single cells to aid in biological research[19–21]. For FLIM, microfluidics can offer a consistent focal plane on the cells, reduce fluorescence crosstalk and background from cell aggregation, and aid image analysis by having predictable cell trapping arrays. Most importantly, microfluidic single cell arrays are excellent platforms to study cell to cell variability (cellular heterogeneity), a topic scientists have begun to realize its importance[22]. In association with microfluidic technology to perform single cell trapping array, FLIM can thus result as a powerful rapid, noninvasive, and label-free method to measure single cell metabolic states.

In this investigation, we employ the use of FLIM to study the effect of aging on the metabolic states of dendritic cells to reveal the possible mechanism controlling age related immunogenic response. Further, we cross correlate the FLIM data with flow cytometry data, which observes for cellular respiratory markers (2-NBDG and Glut-1 PE), to obtain a more complete metabolic profile of DCs. Through understanding the metabolic changes in dendritic cells with age, we hope to explain age related immunosenescence from a metabolic perspective and open research interests in further studying this area.

1.3 Scope of Report

This report details the purpose, motivation, design, results, and discussion of the metabolic profile of dendritic cells found in aged and young subjects. The report provides an overview of the relevant research pertaining to aging, dendritic cells, metabolism and their relationship to the immune response and each other. The report also covers relevant technical background on microfluidic, FLIM, and flow cytometry and how these technologies are relevant

to this study. Methodology on the experimental design, set up, and device fabrication are then detailed. The report will include the resulting findings, data, and the discussion of the effect of aging on the metabolism of dendritic cells. This report concludes with the summary of this text as well as the limitation, future work, and potential application of this study.

1.4 Summary of Conclusion

The results from this study did not yield statistically significant differences in means between aged and young subjects' DC metabolic profiles. Our LPS agonist positive controls behaved as expected, yielding lowered fraction of bound NADH in activated dendritic cells in both aged and young subjects. However, disregarding statistical significance, aging subjects' DCs displayed an interesting trend toward higher ratio of bound NADH over free NADH compared to young subjects' DCs. The result was contrary to our hypothesis and hint that other age related mechanism may be more prominent in controlling the metabolism of DCs than inflammation. We look to repeat the experiments more times to yield a more accurate representation of the truth but nonetheless provide a first look on the difference in metabolism between young and aged subject's dendritic cells.

CHAPTER 2: BACKGROUND

2.1 Aging and Immunosenescence

With the ever-increasing global life expectancy and population of the elderly (post-age of 60 for our study), understanding the aging process has never been more important[23]. Age associated physiological decline can lead to an assortment of degenerative disorders such as cardiovascular, renal, mental, and immunological diseases[4,24–26]. Evolutionary theory accredited aging's deleterious effects to the declining force of natural selection with age. As extrinsic hazards (e.g. predation, accidents, starvation, infection...etc.) reduce the aging population overtime, undesirable late acting genes and alleles were not effectively selected out[27]. One such undesirable aging effect of interest to this study is immunosenescence. Immunosenescence is defined as the gradual degradation of the immune system with age. It is believed to be responsible for a host of pathologically significant health problems in the aging population[26]. Immunosenescence increases susceptibility to infectious diseases and decreased effectiveness in vaccination[28]. Moreover, a hallmark sign of immunosenescence is that of a low grade, systemic, chronic inflammation that can lead to tissue degradation among other complications[2]. This age related chronic inflammation is often termed as "inflammaging," lead popular by Francheschi *et al.* in their landmark paper on immunosenescence[5].

While transient, acute inflammation can be beneficial in combating injury and pathogens, chronic inflammation introduces sustained cellular stress and thus damage to structural and cellular elements of tissue.[2]. In fact, Campisi *et al.* claimed that "most if not all age-related diseases share an inflammatory pathogenesis"[2]. While the causes for inflammaging are not certain, couple theories on the source of this chronic inflammation have been propose. One theory suggests that the accumulation of "self-debris" with age from inadequate elimination of undesirable waste from cells could cause activation of the immune response. The debris could arise from reactive oxygen species (ROS), cellular damage, protein, and metabolite aggregation overtime. The immune system recognizes these debris as dangerous and thus initiate immune response that causes inflammation[2]. Others speculate that cellular senescence initiate inflammation as senescent cells (end stage non-dividing cell) exhibit senescence associated secretory phenotypes (SASP) which include increased secretion of pro-inflammatory cytokines, growth factors, and proteases[29]. There are also theories proposing that unbalanced gut microbiota and genetic predisposition could provide likely explanation of inflammaging[30]. These causes are not conflicting and inflammaging could very well be a combination of these reasons. Regardless of the cause, it is a widely accepted notion that age related chronic inflammation exists and plays an important role in age related diseases.

"Inflammaging" related diseases include but not limited to chronic obstructive pulmonary disease, cancer, maculopathy, osteopenia/porosis, Alzheimer's, Parkinson's, and rheumatoid arthritis[31–40]. In sarcopenia, inflammaging is proposed to contribute to the pathophysiology of the disease through raised levels of pro-inflammatory cytokines: interleukin 6 (IL-6), TNF-α, and C-reactive proteins (CRP)[41,42]. Evidence links high serum IL-6 and CRP levels to threefold increase in risk of grip strength loss over three years. Moreover, IL-6 is known to induce insulin resistance that suppresses muscle synthesis[43]. In frail old subjects, raised expression levels of TNF-α mRNA and proteins were observed in monocytes. TNF-α increases the generation of pro-sacropenic cytokines, mainly cortisol and enzyme 11βHSD1[44]. Vice versa, dampening of inflammatory pathways using glucocorticoid have shown to preserve muscle mass. As such,

these observations are compelling evidences to associate inflammaging to the cause of degenerative muscle loss due to aging. Similarly, in neurodegenerative diseases, Giunta *et al.* have linked inflammaging as a precursor to Alzheimer's disease[45]. Studies *in vitro* and *in vivo* have suggested that pro-inflammatory cytokines such as IFN-γ stimulates the production of amyloid-β, the main component of amyloid plaques found in Alzheimer patients[45]. For osteoporosis patients, an increased CRP level is associated with a 24-32% increase in fracture risk[46]. The heightened levels of IL-6, TNF-α, and TNF receptors also predict a higher chance of non-traumatic fractures[46]. In animal models, blockade of TNF-α and IL-1β have been shown to be effective in treating osteoporosis.

While all these evidences strongly correlate age related inflammation to different diseases, it's important to note that the exact etiology still needs to be further studied. The consensus, however, is that inflammaging heightens the release of pro-inflammatory cytokines TNF-α and IL-6 among others that are strongly associated with disease pathogenesis over a long period.

2.2 Dendritic Cells

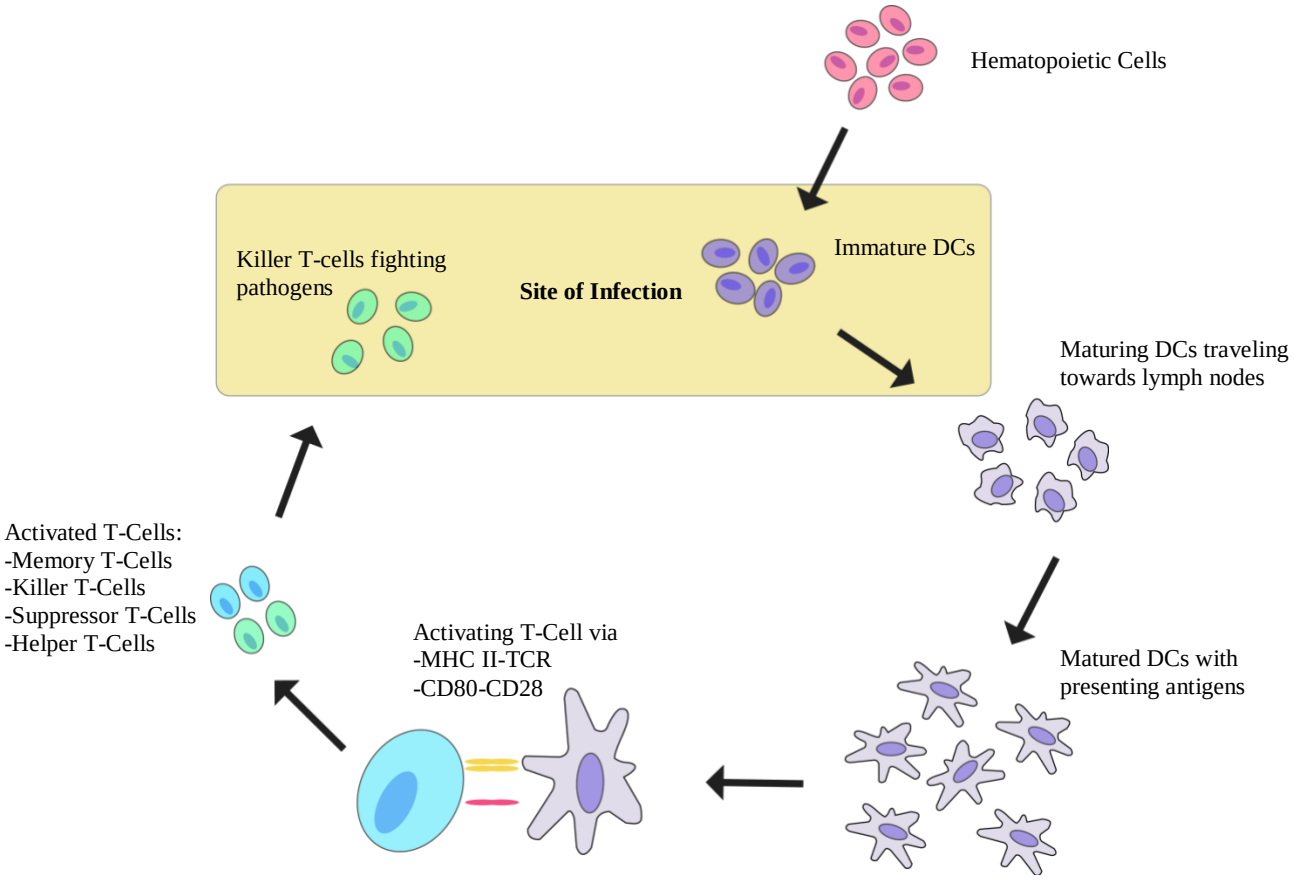

Figure 1: Adaptive Immunity. Immature dendritic cells first differentiate from Hematopoietic cells from bone marrow. Once immature DC encounters pathogens, they mature as they migrate towards lymph nodes to activate T-cells. At the lymph nodes, dendritic cells present pathogenic antigen to matching T-cells including killer T-cells, helper T-cells, suppressor T-cells, and memory T-cells. Killer T-Cells travels to the site of infection to "kill" the pathogens.

Table 1: Dendritic cell subsets and their corresponding characteristics and functions[8].

DC Cell Types	Relevant Phenotypes	Major Cytokines	Toll Like Receptors	Primary Function
Conventional DC (cDC)	$CD1c^{+}$	IL-6	TLR1	Preferentially prime $CD4^{+}$, $CD8^{+}$ T Cells
	$CD11c^{+}$	IL-10	TLR2	
	$CD141^{++}$	IL-12	TLR3	
	$CLEC\text{-}9^{+}$	TNF-α	TLR4	
	$HLADR^{+}$		TLR5	
	$HLADR^{++}$		TLR6	
			TLR8	
			TLR9	
Plasmacytoid DCs (pDC)	$CD303^{++}$	IFN-α	TLR7	Fight Viral Infections and prime $CD4^{+}$, $CD8^{+}$ T Cells
	$CD304^{++}$	IFN-β	TLR9	
	$CD123^{++}$	IL-6		
	$HLADR^{+}$			
Monocyte-Derived DCs	$CD11c^{+}$	IL-6	TLR 1	Prime CD4+, CD8+ T Cells
	$CD14^{-}$	IL-12	TLR 2	
	$HLADR^{+}$	TNF-α	TLR 3	
		IL-10	TLR 4	
			TLR 5	
			TLR 6	
			TLR 8	

At the forefront of immunity are dendritic cells. Dendritic cells are antigen-presenting cells (APC) of the mammalian immune system and can be found in blood as well as mucosal surfaces such as the inner lining of nose, lung, stomach, intestines[47]. Dendritic cells are categorized in four main groups: conventional DC (cDCs), plasmacytoid DCs (pDCs), Langerhans cells, and monocyte-derived DCs (Table 1)[48]. These are a diverse but related group of hematopoietic cell types that expresses various pattern recognition receptors (PRR). Pattern recognition receptors include toll-like receptors (TLR), nucleotide-binding oligomerization domain (NOD)-like receptors, retinoic acid-inducible gene I (RIG-I) receptors, and C-type

lectins. As dendritic cells constantly sample their surrounding environment, PRRs allows immature dendritic cells to recognize pathogens such as viruses and bacteria[49–51]. Once the pathogens are recognized, dendritic cells phagocytose the pathogens and degrade their proteins to present the fragments on their cell surface with major histocompatibility complex (MHC). Often the process of maturation is also referred to as the activation of dendritic cells as they undergo dramatic morphological, secretory changes. During this time, dendritic cells upregulate T-cell co-receptors such as CD80, CD86, and CD40 to prime antigen specific T-cells. Moreover, through the upregulation of CCR7, dendritic cells induce chemotactic receptors that allow DCs to move through the bloodstream to lymph nodes where DCs can activate the helper T-cells, Killer T-cells, and B-cells (Figure 1).

Monocyte derived dendritic cells (MDDC) are the subset of dendritic cells used in this study. Monocytes originate from bone marrow and enter the blood streams to circulate in the body. During infection, monocytes differentiate themselves into different types of macrophages to perform different functions[52]. One of the subsets of cells monocyte can potentially differentiate into are dendritic cells[53]. *In vitro,* these MDDCs are much easier to isolate than *ex vivo* isolated human DCs and thus allowed for various studies to be done on human dendritic cell differentiation and maturation[53]. Human monocyte cultured with GM-CSF and IL-4 allows monocytes to differentiate into immature DCs in a process that takes around 6 days. These differentiated immature DCs have low expressions of costimulatory molecules, MHC II, and do not proliferate further. To activate immature MDDCs, known agonist such as LPS, TNF-α, IFN-γ, or CD40L can be used for DC activation. Once activated, these DCs upregulate costimulatory molecules, MHC II, and display dramatic changes in antigen presentation, chemotaxis behaviors, and their ability to prime and modulate T-cell, NK-cell, and B-cell immune response. However, it's important to note that *in vitro* MDDC studies cannot faithfully replicate *in vivo* MDDC behaviors[53]. Nonetheless, *in vitro* MDDC can be a useful tool in providing valuable information on DC related physiological processes. In fact, current immunotherapeutic treatments for cancer uses *in vitro* MDDCs[54].

Studies on the effects of aging on dendritic cells have yielded different conclusions but together supports the notion that aging dramatically affects DC behaviors and functions[28]. In terms of the relation between DC cell number and aging, there are conflicting reports on the overall DC cell count with age. Della-Bella *et al.* reported a decline of in the number of mDC as well as their CD34+ precursors[55,56]. However, Steger *et al.* and others have reported no differences in DC cell count instead[57,58]. Studies from our lab yielded no significant difference in cell count between aged and young subjects[10]. As for DC function and cytokine secretion, there's a marked increase in pro-inflammatory cytokines (IL-6, TNF-α) with age with a decrease in cellular functionality[9,10]. In summary, aged monocyte-derived DCs shown a decrease phagocytosis and migration activity and decreased expression of IL-10, IFN-α, and IFN-λ secretion[59–61]. IL-10 is the anti-inflammatory cytokine and acts as a negative feedback loop for inflammation through downregulation of Th1 cytokines, MHC class II antigens, and co-stimulatory molecules. Like previously mentioned, IL-6 and C-reactive protein are pro-inflammatory cytokines are also often associated with age related diseases such as type-2 diabetes, rheumatoid arthritis, and osteoporosis, congestive heart failure, and arteriosclerosis[62–66].

2.3 Metabolism and Its Role in Immune Response

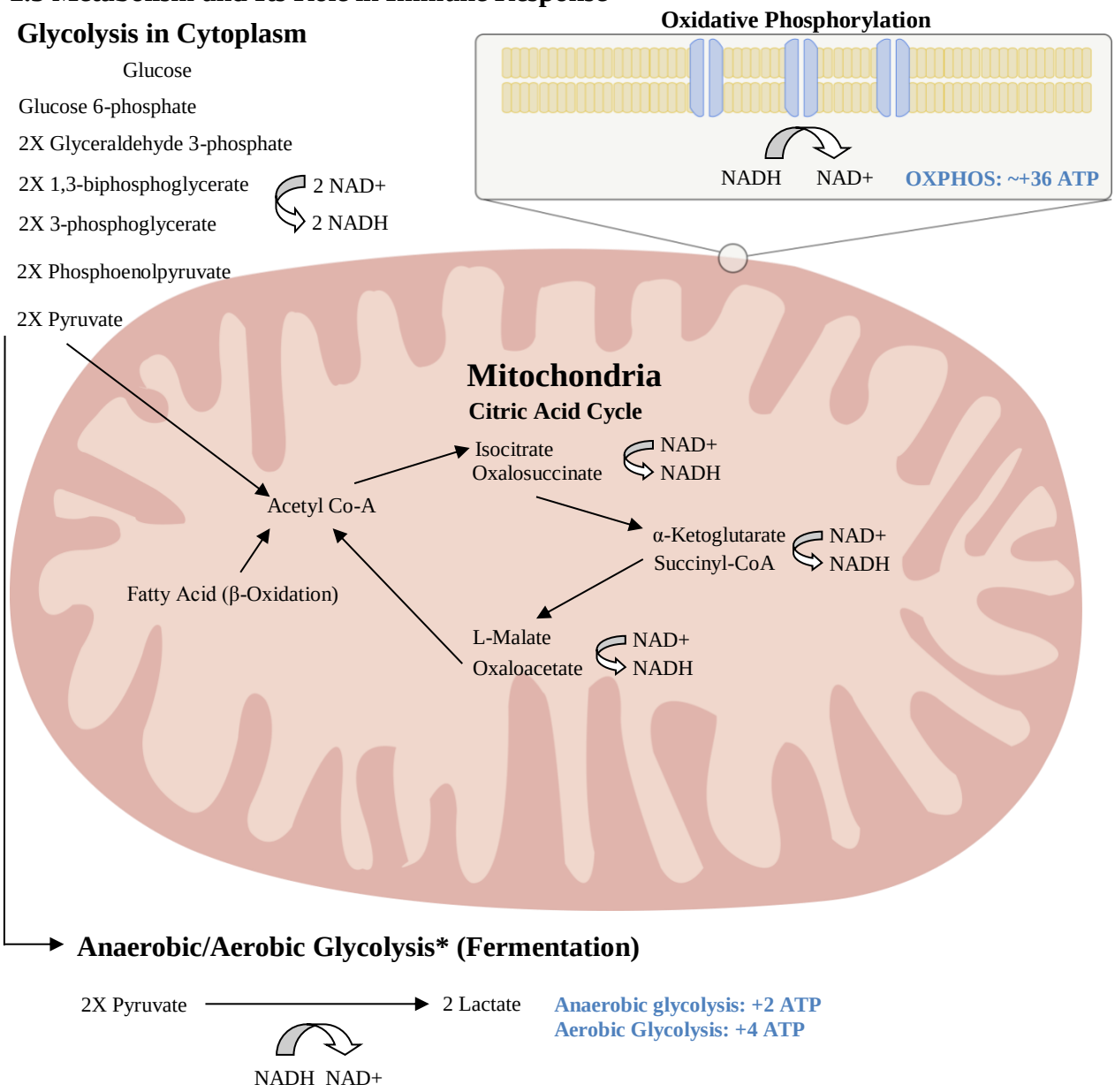

Figure 2: Cellular Respiration Pathways[18]. The figure describes the pathways glucose enters to generate ATP. *Aerobic glycolysis is a special pathway where fermentation occurs in presence of oxygen.[67]

Metabolism consists of the biochemical process in which an organism generates or consumes energy. Almost every function of the cells involves metabolism to a certain degree[68]. As such, considerable efforts have been put into understand metabolism with 15 Nobel prizes awarded in metabolism related research[69]. Cellular respiration is a host of metabolic processes and reactions occurring within the cell to produce adenosine triphosphate (ATP) (Figure 2). These metabolic reactions are catabolic processes that breaks down nutrients to produce chemical energy for the cell. In Eukaryotes, mitochondrion is an organelle that governs cellular metabolism and is closely linked with the proper functioning and overall health of the organism.

In humans, mitochondria dysfunction is linked to a variety of diseases including neurodegenerative, cancer, diabetes, and aging[70].

There are two main cellular respiration pathways, anaerobic (without oxygen) and aerobic (with oxygen). Briefly, metabolism occurs when nutrients such as carbohydrates, proteins, fats are broken down into glucose and enters the glycolysis pathway in the cytosol of cells. In aerobic conditions, glucoses are decomposed into two pyruvates netting two molecules of ATP. Pyruvate are then oxidized to form acetyl-CoA of which enters either the aerobic or anaerobic respiration. If oxygen is present, Acetyl-CoA enters the 8 step Krebs cycle that involves 19 different enzymes. From that cycle, NAD is reduced to NADH, which is used in the electron transport chain/oxidative phosphorylation in the mitochondria. There, NADH is oxidized to generate the chemiosmotic gradient change that drives ATP production. The end yield from one glucose from aerobic respiration is 30-36 ATP. In anaerobic respiration, glycolysis generates NAD+ through pyruvate reduction into lactate. This process usually occurs under hypoxia conditions to generate energy even when there is no oxygen. This process is also especially useful under short, high cellular demands as NAD+ can regenerate fast enough to maintain energy production[71,72]. However, increased acid production from the upregulation of anaerobic glycolysis results in micro-environmental acidosis, which can be toxic to cells[67].

There is, however, one additional pathway named aerobic glycolysis. This process occurs when glycolysis converts glucose into lactate even in the presence of oxygen. The effect is first observed in cancer cells by Nobel laureate Otto Heinrich Warburg in 1924 when he demonstrated that cancer cells increases uptake of glycolysis to meet their bioenergetic needs, regardless if the cells have oxygen or not. It was previously thought that these cells were under hypoxia conditions or that the mitochondria were damaged and thus the cells adapted to aerobic glycolysis. However, recent studies have shown that these cells employ aerobic glycolysis to initiate proliferative PI3k/AKT/mTOR as well as AMPK pathways. These pathways facilitate the uptakes of nucleotide, amino acids, and lipids to allow for cells to metabolize them for growth and proliferation[68].

Interestingly, in dendritic cells, TLR agonist driven activated DC have shown to adopt aerobic glycolysis as well[11]. In murine model, Everts *et al.* shown that within minutes post activation with TLR agonist, increased glycolysis occurs in CD8+α and CD11b+ cDCs[13]. Treated with 2-deoxyglucose, a glycolysis inhibition enzyme, DCs activation are inhibited and thus support the finding that glycolysis is vital to the activation of DCs. In fact, in bone marrow derived DCs, activation with TLR agonists for more than 12 hours have shown to shut off the oxygen phosphorylation pathway[13,14]. As to the reason for the adoption of glycolysis in activated DCs is not yet entirely clear. However, the transport of pyruvate using MPC1 into the mitochondria is essential to the activation of DC. Thus, it has been proposed that the increased glycolysis in activated DCs is used to fuel the TCA through the increase production of pyruvate. TCA cycle increases fatty acids production which is linked to the enlargement of endoplasmic reticulum and Golgi. The enlargement of these organelles allows for the increased synthesis of protein by the activated DCs[11].

2.4 Fluorescence Lifetime Imaging Microscopy

Fluorescence Lifetime Imaging Microscopy (FLIM) measures the rate of the fluorescence exponential decay from a sample post-excitation of a photon. The fluorescence lifetime (τ), in practice, is measured as the time for the fluorescence intensity to decay to 1/e of its original

intensity (I_0) post excitation. As different molecules exhibit different fluorescent lifetime signatures, FLIM can be used as a high sensitivity method to measure the relative abundance of a molecular specie from a sample[73]. There are a wide variety of FLIM set up as multiple factors such as light source, optics, and techniques to obtain lifetime could all differ. For our study, we use two-photon microscopy to excite free and bound NADH molecules. Two-photon have inherent sectioning effect through the result of point spread function. This allows two-photon to excite the plane of focus thus eliminating substantial background noise[74]. Moreover, the near infrared wavelength of two-photon excitation allows for deeper penetration depth and cause less cellular damage compared to the shorter wavelengths lasers typically employed by single photon lasers[17]. Hence, two-photon microscopy serves as a high resolution, long term biological imaging solution appropriate for this study.

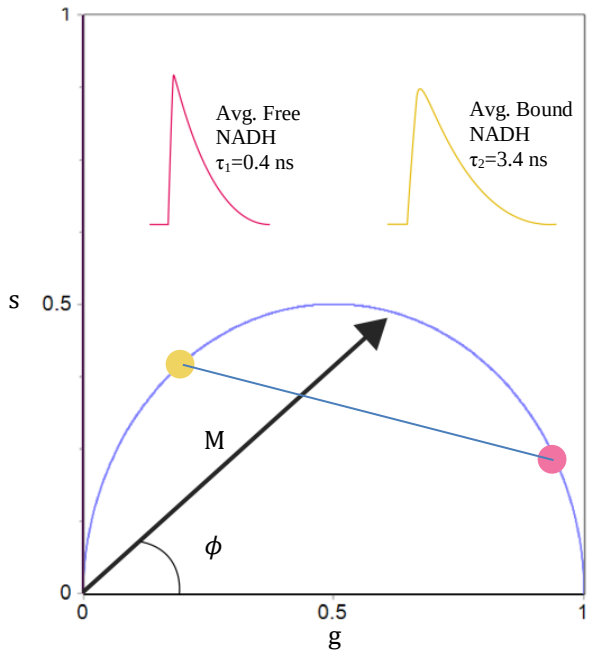

Figure 3: Transformation of fluorescence lifetime decay curve into phasor plot.

$$I(t) = I_0 \cdot \exp(-\frac{t}{\tau}) \qquad \text{Eq. 1}$$

For analyzing FLIM results, one analytical method to provide straightforward FLIM information is to Fourier transform the fluorescence lifetime decay (Eq. 1) and plot the resulting complex number on a phasor plot (Figure 3). This method is also known as the phasor-FLIM approach.

$$g_{i,j}(\omega) = \frac{\int_0^\infty I_{i,j}(t)\cos(\omega t)dt}{\int_0^\infty I_{i,j}(t)dt} \qquad \text{Eq. 2}$$

$$s_{i,j}(\omega) = \frac{\int_0^\infty I_{i,j}(t)\sin(\omega t)dt}{\int_0^\infty I_{i,j}(t)dt} \qquad \text{Eq.3}$$

Above shows the Fourier transformation of time-domain data from each pixel (i,j) (Eq. 2, Eq. 3). ω corresponds to $\omega = 2\pi f$, where f is the laser frequency (80 MHz in this study). $g_{i,j}(\omega)$ and $s_{i,j}(\omega)$ represents the X and Y coordinate respectively on the phasor plot. Consequently, a unique position on the plot corresponds to a unique molecular fluorescence lifetime signature from a pixel of FLIM image. This method eliminates the need for multi-exponential analysis of the lifetime of the phasor since all possible lifetime will fall within the semicircle (Figure 3)[73]. As such, plotting the Fourier transformed decay curve on phasor plot allow lifetimes to be easily estimated and visualized.

For the fluorescence decays of multiple components (e.g. dendritic cells), the fractional summation of each phasor component is calculated (Eq. 4, Eq. 5):

$$G(\omega) = \sum_1^n f_n g_n(\omega) \qquad \text{Eq. 4}$$

$$S(\omega) = \sum_1^n f_n s_n(\omega) \qquad \text{Eq. 5}$$

With phasor-FLIM, vectorial superposition of multi-species decay curves is possible through the generation of the linear line connecting the phasors of the different individual species' decay. For example, in our study, the mixtures of protein bound NADH decay and free NADH decay should result in phasors lying on the line generated by the two points from phasor of the species (Figure 3).

As such, with phasor-FLIM, analysis of the relative abundance between protein bound NADH and free NADH within a cell can be easily calculated. In 1992, Lakowicz *et al.* first demonstrated the possibility of obtaining lifetime images from free and bound NADH[16]. NADH belongs to a class of intrinsically fluorescence molecules found in live tissues and cells. These molecules include endogenous proteins and fluorophores such as elastin, flavins, hemoglobin, serotonin, and NADH to name a few[75]. Hence these molecules have been extensively used by FLIM to study different cellular behavior, differentiation, and carcinogenesis phenomena[76–79]. Since NADH is a prominent co-enzyme in metabolic processes described above, monitoring the metabolic pathway the cell takes can thus be feasible through FLIM techniques. During glycolysis, free NADH is produced as a product to generate the potential gradient of the electron transport chain. However, during oxygen phosphorylation, NADH is oxidized to NAD^+ and thus changing the enzyme kinetics to produce higher ratio of bound NADH[18,78]. Using the fact that free and protein-bound NADH displays a lifetime of around 0.4 ns and 3.2 ns respectively, phasor-FLIM can extract the ratio between the two molecular species and thus deduce the dominant metabolic pathway useful for this study[18,78].

2.5 Microfluidic Background

Device miniaturization has been one of the key advancement in recent times. In semiconductors, Moore's law claims that the number of transistors per square inch will double every two years. Similarly, in life sciences, albeit less dramatic, there's a push towards miniaturization. However, the reduction of reagent and reactions volumes have often been limited by the effects of evaporation and "wicking" of capillary action[80]. These limitations severely restrict the ability to precisely handle small volumes in traditional microtiter plate settings. As a result, recent advancements in microfluidic proves to be a promising field that allows for the manipulation of small volumes of liquids and gases in an accurate and portable manner. With micro-size channels, microfluidics lowers the Reynolds number to produce

laminar flow that's predictable and easier to control[81]. Microfluidics devices also usually use less amounts of samples and reagents compared to benchtop methodologies while providing higher sensitivity and quicker result turnaround times. Moreover, parallelization, automation, and integrations of different techniques is possible on microfluidics and has been demonstrated in a wide variety of applications[82]. For these compelling reasons, microfluidics has begun to gain traction in biological sciences to manipulate, simulate, or analyze biological substances such as organs, cells, and DNA[82].

Single cell microfluidic platforms have recently become an area of interest as researchers began to understand the importance of cellular heterogeneity (cell-to-cell variability). Cellular heterogeneity became important when several studies reported that individual cells from the same batch displays different genotypes and phenotypes even under identical environments and conditions[83]. To combat cellular heterogeneity, a multitude of microfluidic designs have been developed for single cell trapping. Single cell traps can be categorized in these three major designs: serpentine[19,20,84–87], Di Carlo method[21], and droplet microfluidics[88–90]. Serpentine method works on the principle of hydrodynamic confinement and the path of least fluidic resistance. Kobel *et al.* reported that this method can achieve up to 97% trapping efficiency[85]. Di Carlo method traps single cells through cup like arrays with the advantage of incurring lower shear stress on the cell compared to the serpentine channels[91]. Lastly, droplet fluidic also present an attractive method with high throughput cell trapping through emulsion droplet. However, droplet microfluidics is more complicated to set up as it requires the use of fluorinated oil and prevents further downstream cell processing[89].

Recently from our lab, Xuan *et al.* reported a high density serpentine channel single cell trap used for *in situ* mRNA extraction with AFM probe[20]. Lee *et al.* employed a similar trapping array system to perform FLIM identification of leukemia cells[19]. The reported design has size selective traps to filter out unwanted red blood cell from diluted whole blood while achieving near 70% single cell trap efficiency. As such, taking advantage of the already in house optimized serpentine device, we adapted the platform to fit the application of dendritic cell trapping for FLIM imaging. Mature DCs ranges from 10-15 μm in size while immature DC ranges from 6-9 μm[92]. In this study, we used 15 μm size width traps with a gap height (hg) of 4 μm (Figure 5). Theoretically, this design should be able to trap any cells under the size of 15 μm, including both immature and mature dendritic cells. We did also attempt to fabricate variable width size traps from 7-20 μm with the hope of increasing single cell capture efficiency. Due to fabrication hurdles and time constraints, the device was not completed. Nevertheless, single cell trapping is not the focus of the study but rather as a tool to aid FLIM imaging and analysis.

Microfluidic can substantially benefit imaging in FLIM because of how the channels can be designed to fit the size of the cells and trap cells in predictable manner. With traditional imaging dish cell culture, FLIM suffers from potential background and cross talk from cell aggregation. As mentioned previously, 2-Photon FLIM have inherent sectioning effect on the Z-plane. This also means that controlling an even height of which the cells can be imaged can be difficult and thus leads to potential result variability. Purpose built microfluidics can alleviate much of the height problem by designing channel heights that allows only one cell to path and trap. Moreover, trapping cells in arrays allow for ease of image capturing and processing as cells can be located at predictable areas. Lastly, the trapping array separates much of the cells away from each other, reducing fluorescent signal bleed to provide better SNR.

2.6 Flow Cytometry

Flow Cytometry is a highly established field of research with several competing commercial products on the market. The technology has origins dating back to the early 50's. First patented by Wallace H. Coulter in 1953, the Coulter principle uses the change in impedance to count and size particles flowing through an orifice. As cells are poorly conductive particles, they raise the electrical resistance thus decrease the electric current when they pass through the channel. Through observing the changes in electrical current, the size and number of cells can be deduced accordingly. Fifteen years later in 1968, the first fluorescence-based flow cytometer was patented by Wolfgang Gohde. Briefly, in modern fluorescent flow cytometers, a laser light source excites samples usually stained with fluorescent molecules that either binds to proteins or ligands of interest. The flow cytometer then reads the emission from the fluorochromes as well as the forward and side scatter from the light beam as the cell passes through the light. The forward scatter measures the cell size while the side scatter correlates with cellular granularity. Since then, the device has been continuously improved to become faster, more multi-parametric, and more robust. As a result, the device today is a powerful tool to perform single cell analysis in a high throughput manner (up to thousands of cells per second).

To monitor glycolytic activity in our dendritic cells, two fluorescent markers were used for this study: 2-NBDG and Glut-1. 2-NBDG or (2-deoxy-2-[(7-itro-2,1,3-benzoxadiazol-4-yl)amino]-D-glucose) is a fluorescent glucose analog used to detect "direct glucose uptake" by cells[93]. Through the use glucose transporter, 2-NBDG is taken up by the cell and phosphorylated by hexokinase[94] (TeSlaa 2014). Therefore, 2-NBDG can acts as a fluorescent biomarker for cellular glycolytic flux. To excite 2-NBDG, 465 nm wavelength light is used as excitation source. 2-NBDG emits 540-nm wavelength light which can be detected using a fluorescein filter (530/30). Similarly, Glut-1 PE-conjugated antibody marks for glucose transporter 1 (GLUT1) expression in the cell. GLUT1 transport glucose across the plasma membrane and is the most widespread glucose transporter. Metabolic changes and oxidative stress have shown to affect GLUT1 expression levels[95]. Moreover, Cho *et al.* demonstrated that aged induced fibrogenesis is linked to increased GLUT1 dependent glycolysis[96]. As such, GLUT1 is also a viable marker to monitor glycolysis activity. GLUT1 PE, as the name suggests, can be observed in phycoerythrin channel (585/42) with a peak emission wavelength of 575 nm and an excitation wavelength of 488 nm.

Through monitoring both 2-NBDG activity and GLUT1 expression, we can obtain an overview of glycolytic uptake and activity. It is important to mention that these markers do not reveal the downstream fates of the glycolytic derivatives (e.g. oxidative phosphorylation or anaerobic glycolysis) but the results from FLIM should instead show that information. Thus, by combining FLIM with flow cytometry data, we can have comprehensive view on dendritic cells' cellular respiration and metabolic profile.

CHAPTER 3: RESEARCH DESIGN AND METHODS

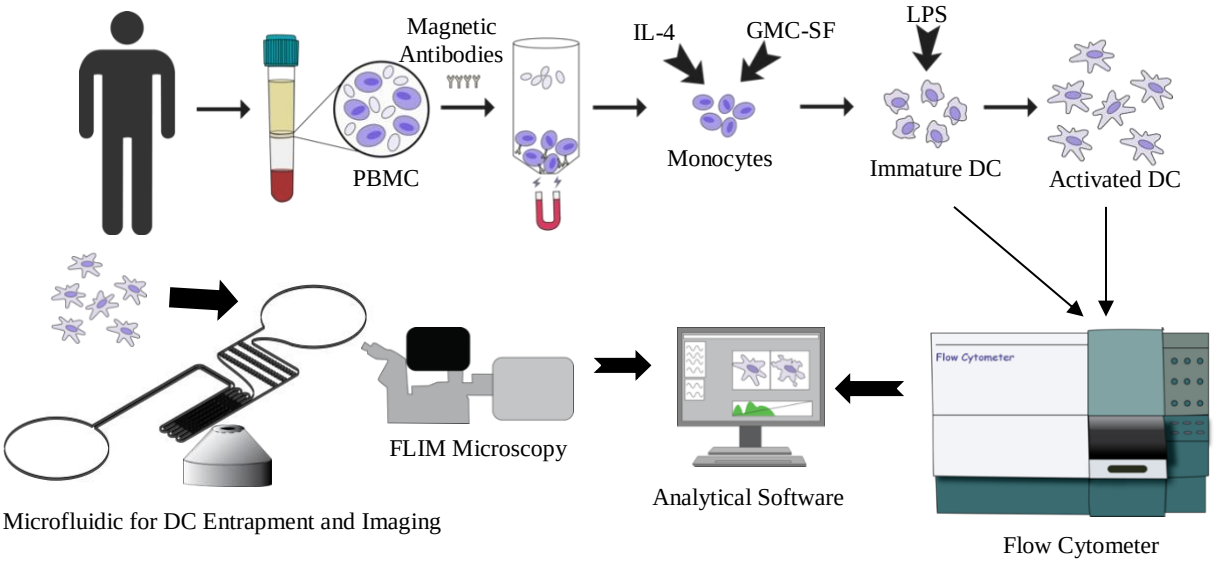

Figure 4: Overview of dendritic cell isolation, imaging, and analysis. Briefly, monocytes were isolated from human donors' blood. Then, monocytes were given differentiating cytokines to allow them to differentiate into dendritic cells (DC) with of the DCs given LPS for activation. DCs metabolism were analyzed using flow cytometry and FLIM Microscopy. For flow cytometry, DCs were stained with 2-NBDG and Glut1 PE.

3.1 Subjects, Cell Preparation, and Viability Assays

Subject human blood was obtained from UCI General Clinical Research Center with Institutional Review Board, University of Irvine approval. Donors were categorized as young and aged (Subjects n=16, 9 young, 7 aged). Young subjects ranges from age 21-38 and aged subjects ranges from age 60-78. Peripheral Blood Mononuclear Cells (PBMC) were isolated using Lymphoprep™ (STEMCELL Technologies) through density gradient centrifugation. Lymphoprep™ to blood ratio is 1:2 with added 1X HBSS. The tubes are centrifuged at 2000 RPM for 15 minutes with brakes off. PBMC layer were extracted from the tubes using a pipette. The PBMCs were then centrifuged at 2000 RPM for 5 minute with brakes on and centrifuged again at 1000 RPM for 5 minutes with brakes off in polystyrene tubes. The PBMC cells were resuspended per vendor protocol with CD14 positive selection antibody (EasySep™ Human CD14 Selection Cocktail II; STEMCELL Technologies) used to capture desired monocytes with dextran coated magnetic bead (EasySep™ Dextran RapidSpheres™ 50100; STEMCELL Technologies). The mix of labeled cells were put in EasySep™ magnet for 2-3 minute before the unwanted cells were poured out. The desired cells were resuspended in RPMI 1640 (10% FBS, 1 mM glutamine, 100 Ul/ml penicillin, 100 g/ml streptomycin).

With the isolated CD14+ cells (monocytes), monocytes were then differentiated into dendritic cells using 50 ng/ml human recombinant rGM-CSF (Peprotech Inc.) and 10 ng/ml human rIL-4 (Peprotech Inc) in the medium. The cells were cultured over 6 days, with the medium with cytokines replaced every 2 days. For lipopolysaccharide (LPS) activation, DCs were cultured with 1 μg/ml LPS (Sigma-Aldrich) for additional 18-20 hours. Aliquots of the cells from same batch were then used for flow Cytometry and FLIM analysis.

HeLa cells were cultured in Gibco® DMEM medium (Thermo Fisher Scientific) with 4.5 g/L D-Glucose, L-Glutamine and supplemented with 10% FBS and 1% penicillin/streptomycin.

The cells were passaged every 3-4 days using standard sterile protocols and stored in 37ºC at 5% CO_2. Trypan blue assay was used to test cell viability as well as determining cell concentration for both HeLa and DCs. In short, cells in medium were diluted 1:1 with Trypan Blue, 0.4% (Thermo Fisher Scientific) and counted with a hemocytometer or with Countess® Automated Cell Counter (ThermoFisher Scientific) per protocol.

3.2 Microfluidic Device Design and Characterization

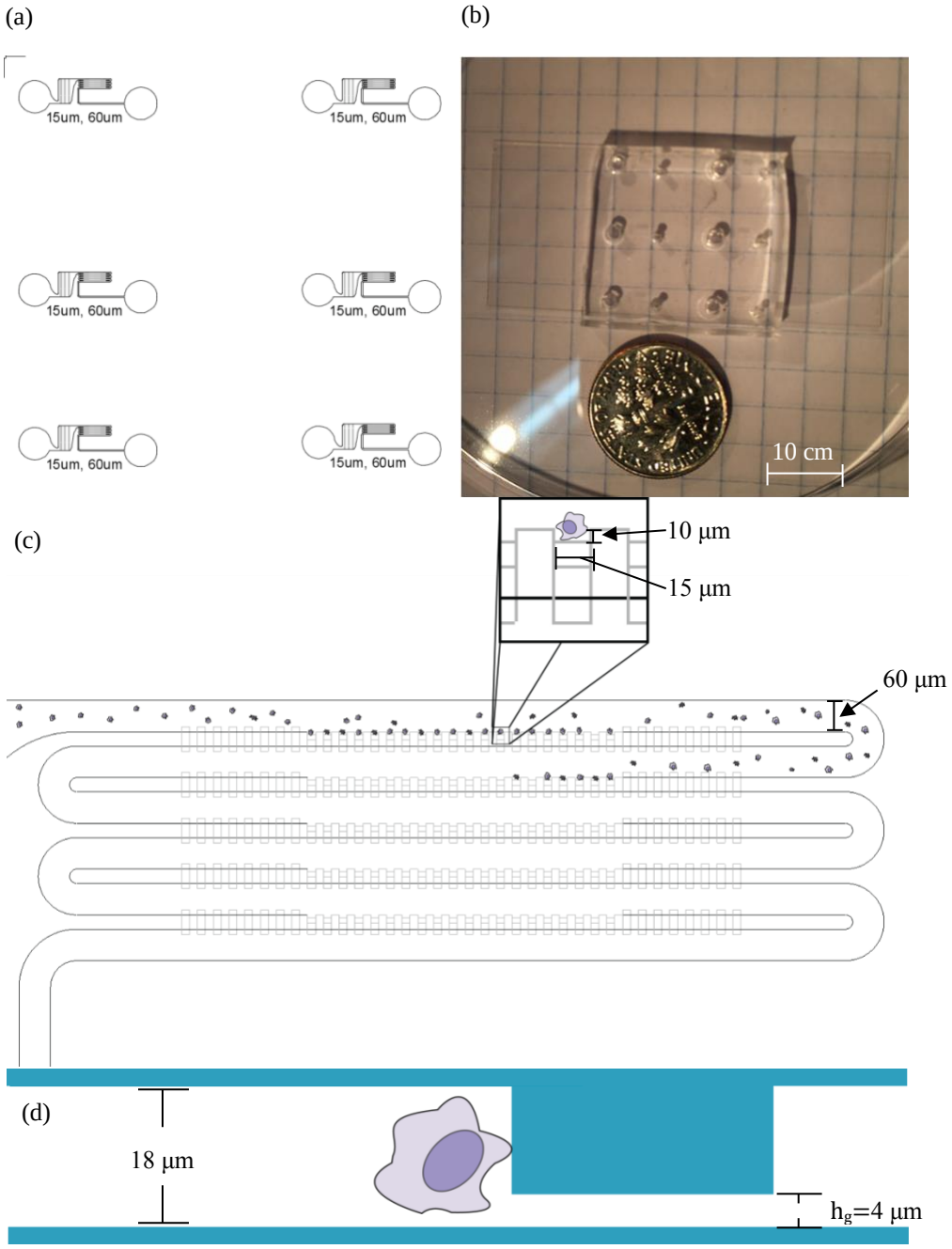

Figure 5: Microfluidic trap design. (a) Array of six cell trapping devices each capable of trapping 100 cells. (b) Array of six devices fabricated in PDMS and bonded to a cover glass, dime for scale. (c) Proposed dendritic cell

trapping mechanism of the microfluidic device with trap size width of 15 μm, length of 10 μm. (d) Side sectional view of the microfluidic device with channel height of 18 μm and a h_g gap of 4 μm.

The serpentine shaped microfluidic device was designed with a channel width of 60 μm and height of 18 μm. Prior to the traps, the cells pass through a filter region to break up the cell clumps. The trap has a dimension of 15μm width, 10 μm length, and 18 μm height. The trap also comes with a 4 μm slit (h_g) to allow for flow to pass through but not the cell (Figure 5). The device is designed with 5 rows, each with 20 traps, allowing the device to trap up to 100 cells.

Finite Element Modeling (FEM) was performed using COMSOL Multiphysics (COMSOL, Inc.). A stationary, laminar flow study was selected with the corresponding microfluidic 3D geometry constructed in extra fine mesh. Material density was set at 1000 kg/m^3, viscosity set at 0.001 Pa·S, and an input flow rate of 5 μl/min. Streamlines were constructed to view the flow of least fluidic resistance.

3.3 Microfluidics Fabrication

The microfluidic device design was made using Autocad 2017 (Autodesk, Inc.). Each layer of the design was printed on a photomask (4x4x0.06 LRC Chrome, 5um Resolution Mask, Protective Poly/Nano 3M coating; FrontRange Photomask, Inc). The mold was produced on a 3'' silicon wafer with standard multistep photolithography techniques[97]. Briefly, the wafer was first placed in HF for 2 minute to remove SiO_2 then dehydrated at 120ºC for 15 minute. SU-8 2005 (MicroChem Corp.) was spun at 4000 RPM for 30 secs, baked at 65ºC for 1 minute then at 95ºC for 2 minute. Using a Karl Suss MA56 mask aligner (Karl Suss America Inc.), the spin-coated wafer was exposed with a UV dosage of 95 mJ/cm^2 through the first layer mask. The exposed-wafer was baked at 65ºC for 1 minute then 95ºC for 3 minutes. The features were then developed for 1 minute in SU-8 developer (MicroChem Crop.). For the second layer, SU-8 2025 was spun on the same wafer at 2700 RPM for 30 secs, baked at 65ºC for 1 minutes, and 95ºC for 3 minutes. After aligning the 2nd-layer mask with the 1st-layer's alignment markers using Karl Suss MA56, the wafer was exposed with a UV dosage of 140mJ/cm^2. Finally, the device was baked at 65ºC for 1 minute, 95ºC for 3 minutes, and developed for 4 minutes.

After the wafer mold was made, 10:1 liquid Polydimethylsiloxane (PDMS) to curing agent was mixed and poured on the wafer mold. The wafer mold with PDMS was degassed for 30 minutes, heat gunned to remove surface bubbles, and then baked at 65ºC overnight to complete crosslinking. The cured PDMS device was then cut from the wafer, punched, and plasma bonded to a 22x50 mm micro cover glass (VWR International). Each cover glass contains 6 individual PDMS cell trap devices. Prior to cell entrapment, 1X PBS was loaded in the device using a pipette to prime the channels.

3.4 FLIM Setup and Data Acquisition

Monocyte derived dendritic cells from the different subjects with and without LPS activation were loaded into the microfluidic device. Approximately 10 μl of $5x10^5$ cells sample was loaded into the inlet punched with a 2 mm biopsy punch (Integra Miltex). As for the outlet, a 1.5 mm punch was used to make a withdraw outlet pumped with PicoPlus syringe pump (Harvard Apparatus). An initial pull of 20 μl/min may be required to initiate the cells to flow into channel and then reduced to 5 μl/min to maintain steady flow. The pumped was turned off when

the traps become saturated with cells. The device was then immediately loaded onto FLIM microscope for imaging.

Fluorescence lifetime imaging microscopy was performed using 2-photon excitation laser coupled to Zeiss LSM 880 scanning microscope (Carl Zeiss AG) and an ISS A320 FastFLIM unit (ISS). The laser is powered by a mode-locked Ti:Sapphire, producing laser pulses at 80 MHz with 140 femtosecond pulse width (Spectra-Physics). To perform 2-photon excitation of free and bound NADH, a 740 nm wavelength laser was used at 2% laser attenuation to produce around 3.2 mW. The laser was focused onto the sample with a 40x, 1.20 numerical aperture, apochromatic water immersion microscope objective lens. The low wattage prevents cellular damage as well as photobleaching of NADH. An external HPM-100-40 high speed detector (Becker & Hickl, GmbH) and a band pass filter of 420-500 nm was used to detect the emission from free and bound NADH. The laser scans at 16.38 μsec per pixel and scans an image with 256x256 pixels per frame. 50 frames were taken per image. Calibration of FLIM was performed using the known lifetime (2.5 ns) of diluted Coumarin-6 in ethanol. Data acquisition and analysis was performed using Globals for Images, SimFCS 3 developed by Laboratory of Fluorescence Dynamics, University of California in conjunction with Zeiss software Zen v2.3 (Carl Zeiss AG).

3.5 Flow Cytometry Setup & Data Acquisition

After monocyte derived dendritic cells were harvested from the different subjects with and without LPS activation, aliquots of the different age groups and their respective conditions were divided up for 2-NBDG and Glut1 staining. For 2-NBDG stain of DCs, cells were first washed with 1X PBS. Then, 2-NBDG were added to the sample to achieve a final concentration of 100-200 ug/ml (Cayman Chemical Company). After incubation for 30 minutes at room temperature, the cells were washed again with 1X PBS and placed in FACS Tubes. The tubes with cells were loaded up in FACSCalibur (BD Biosciences) and excited with 488 nm wavelength laser. The emission was read using the FL-1 channel which has a 530/30 filter. Similarly, for human Glut1 PE conjugated antibody (R&D Systems), cells were washed with 1X PBS and stained per vendor protocol for 30 minutes at room temperature. Then, the cells were washed again with 1X PBS and placed into FACS™ Tubes (BD Biosciences) to be read by FACSCalibur™ (BD Biosciences). Single cell flow cytometry was ran until there were approximately 20,000 cells read per sample condition. Data analysis was performed using FlowJo® v6 (FlowJo, LLC) with histogram and mean calculated.

3.6 Statistical Analysis of Data

Statistical analyses were performed with R (The R Foundation). Fraction of bound NADH values were extracted from each cell using Globals for Images, SimFCS. Data points were then compiled for each subject and condition. Shapiro-Wilk Tests were performed to test for data normality. For normal data, unequal variance Welch's T-Test were used to compared the following conditions: Young vs Young LPS+, Aged vs Aged LPS+, Young vs Aged, Young LPS+ vs Aged LPS+. For non-normal data, Mann-Whitney-Wilcoxon signed-rank test was used for non-parametric statistical analysis for the same conditions.

CHAPTER 4 RESULTS AND DISCUSSION

4.1 Monocyte Derived Dendritic Cell Viability

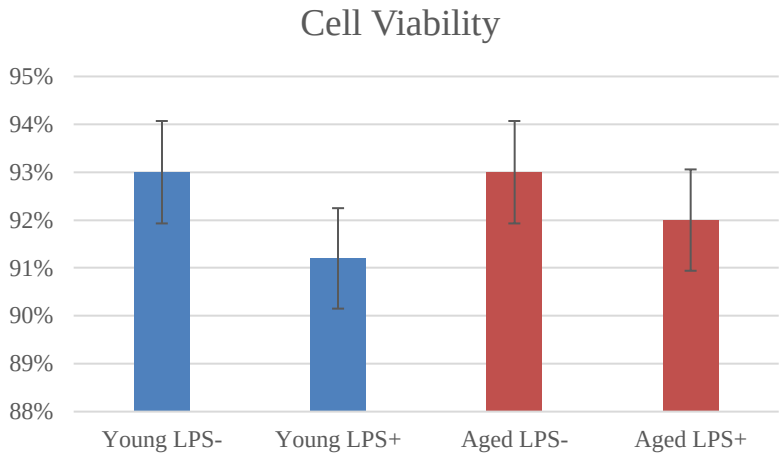

Figure 6: Cell viability across age group and LPS activation (n=3).

Cell viability assays and concentrations were ran using Countess® Automated Cell Counter with an overall cell viability of >90%. There were at most a 2% difference between the age groups and conditions with a standard deviation of around 1% across all conditions (Figure 6). The original intent of the experiment was not meant to elucidate any mechanisms or explain any phenomenon of dendritic cells. The test was used primarily to showcase the cells were cultured well and fit for FLIM experimentation. While not statistically significant, it was interesting to note that the cell viability with LPS on average decreases compared to non-LPS activation samples. The correlation might be a result of increased oxidative stress on the cells with dendritic cell activation leading to cellular apoptosis. As dendritic cells become activated, increased biogenetic needs generate more reactive oxygen species (ROS) from increased mitochondrial activity[98]. This increase in ROS production is linked to the release of cytochrome and other apoptotic proteins[99]. Hence, it's likely that the decreased cellular viability is linked to dendritic cell activation with LPS. Nevertheless, more samples are needed to be tested to draw a more conclusive correlation.

4.2 Microfluidic Characterization

4.2.1 FEM Simulation of Microfluidic Cell Trapping Array

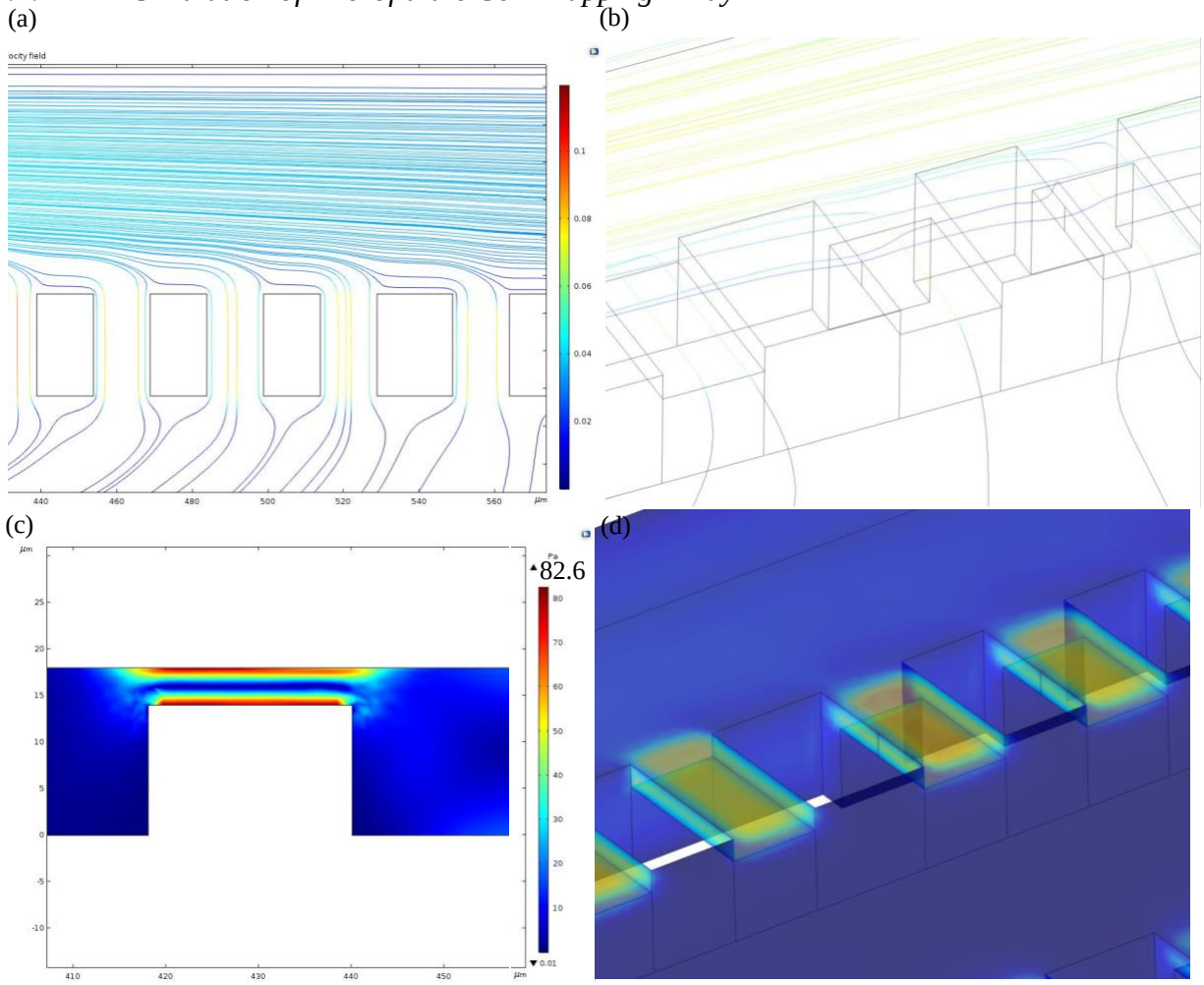

Figure 7: FEM simulation results from COMSOL. (a) 2D streamlines of the device showing fluidic flow taking the path of least resistance. (b) 3D streamlines showing flow through the h_g gap. (c) Cross sectional view of shear stress on the microfluidic device. (d) 3D view of shear stress in h_g gap.

An input flow rate of 5 µl/min (~0.077 m/s flow velocity) was assigned to the inlet of the channels for this FEM study. The simulation inverts the device for the ease of visualizing the results and should not affect the results. As shown in Figure 7 (b), the streamlines enter the cell trapping array and exits through the 4 µm h_g gap. This allows the cells to be trapped effectively into the trap as the cells takes the path of least resistance. The traps closer to the inlet have higher stream velocity than the traps further away. Therefore, the cells have even more hydrodynamic incentive to trap in a sequential order than simply reaching to the traps first. The simulation is consistent with empirical observations we saw. The highest shear stress (82.6 Pa) and flow velocity occurs in the 4 µm h_g gap. There is no data on shear stress and dendritic cell viability as far as we know but according to Mazur *et al.*, macrophages are able to withstand up to ~1,500 dyn/cm^2 (150 Pa) without appreciable fragmentation. Moreover, the viability of macrophages

exposed to 1,000 dyn/cm^2 do not differ to that of the control[100]. Therefore, while it's not desirable for cells to sustain high cellular stress in the h_g gap, our device should still be safe for the cells in the off chance they squeeze through the gap.

4.2.2 Cell Trapping Efficiency

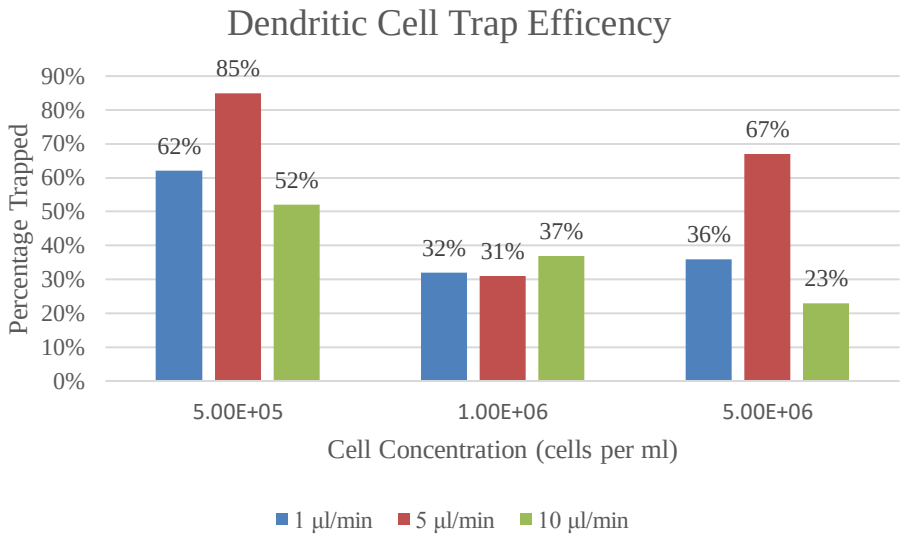

Figure 8: Microfluidic dendritic cell trap efficiency. Percentage of cells trapped at different cell concentrations and channel flow rate.

Table 2: Average percentage of cells trapped with different flow rates.

Flow Rate (µl/min)	Cells Trapped
1	43%
5	61%
10	37%

Table 3: Average percentage of cells trapped with different cell concentration.

Cell Concentration (cells per ml)	Cells Trapped
$5x10^5$	66%
$1x10^6$	33%
$5x10^6$	42%

To assess the efficiency of the single cell array to trap dendritic cells, a simple test matrix with different flow rates and cell concentrations was performed. Intact cells (round) were counted while deformed cells were ignored in this exercise. Multiple cells on traps were calculated as trapped if the morphology of the cells looks intact for FLIM imaging. The highest average cell trapping efficiency for flow rate is at 5 µl/min while the highest trapping efficiency for cell concentration is at $5x10^5$ cells/ml.

4.3 FLIM Results

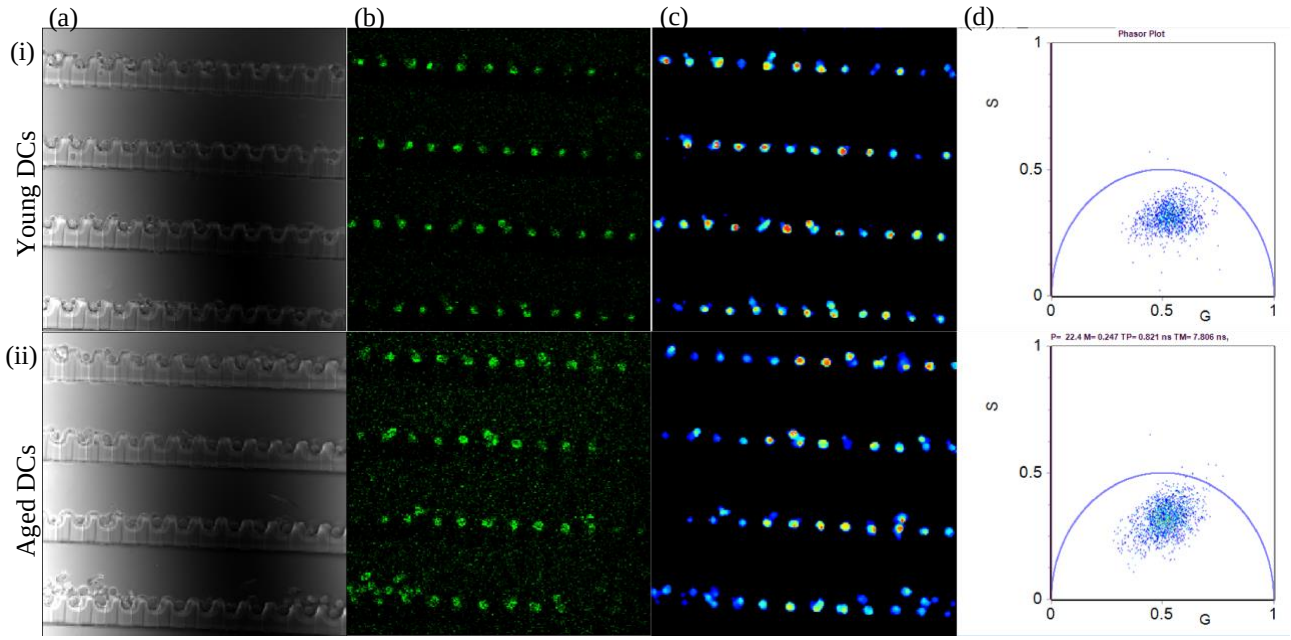

Figure 9: High density microfluidic trapping array FLIM Example. High density microfluidic trapping array used to trap dendritic cells for FLIM Microscopy analysis of Free/Bound NADH. Excited at 740 nm with 2-Photon laser, the detectors capture the emission from free and bound NADH and analyzed using Globals for SimFCS. (i) Young dendritic cell samples (ii) Aged dendritic cell samples (a) Bright field image of cells (b) Live fluorescent Image (c) NADH fluorescence emission intensity image (d) Phasor plot of fluorescence lifetime of the cells.

4.3.1 HeLa Cells shows 2-DG Glycolytic Inhibition with Microfluidic Trapping Array

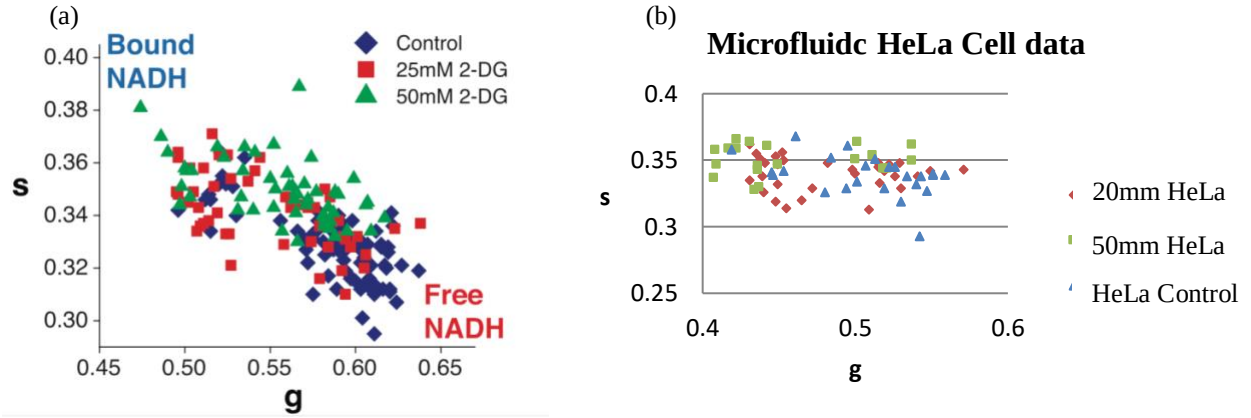

Figure 10: FLIM phasor plot of 2-DG HeLA Experiment. Phasor plot of g and s values comparing (a) previously published FLIM results*[18] (b) to FLIM results on our microfluidic device. **Reproduce with permission from Oxford University Press.*

HeLa cells results from this FLIM study serves as a control to show that cell metabolism shifts toward OXPHOS pathway as cells are exposed to increased concentrations of 2DG. The result is placed next to previously published data performed using an imaging dish[18].

4.3.2 Monocyte Derived Dendritic Cell Free/Bound NADH

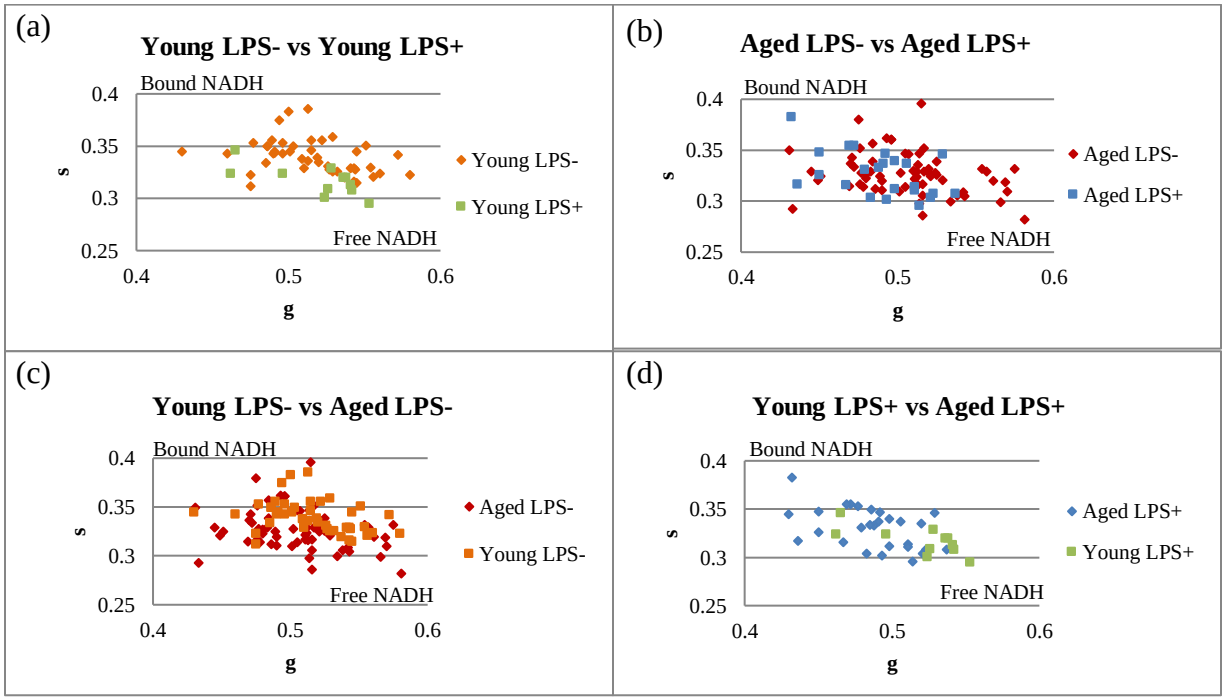

Figure 11: FLIM phasor plot of a dendritic cell experiment comparing different conditions. Note that these data are not indicative of data across all subjects and is meant to show the heterogeneity of the cells. Each point on the graph corresponds to one cell's g and s values. Higher g and lower s values corresponds to more free NADH while lower g and higher s values correspond to more bound NADH. (a) Comparing Young LPS- DCs with Young LPS+ DCs, with more Young LPS+ cells showing more free NADH than Young LPS-. (b) Comparing Aged LPS- DCs with Aged LPS+ DCs, with more Aged LPS+ cells again showing more free NADH than Young LPS-. (c) Comparing Young LPS- DCs with Aged LPS- DCs, Aged LPS- cells have slightly more cells displaying more Free NADH. (d) Comparing Aged LPS+ DCs with Young LPS+ DCs. Young LPS+ DCs shows more free NADH than Aged LPS+.

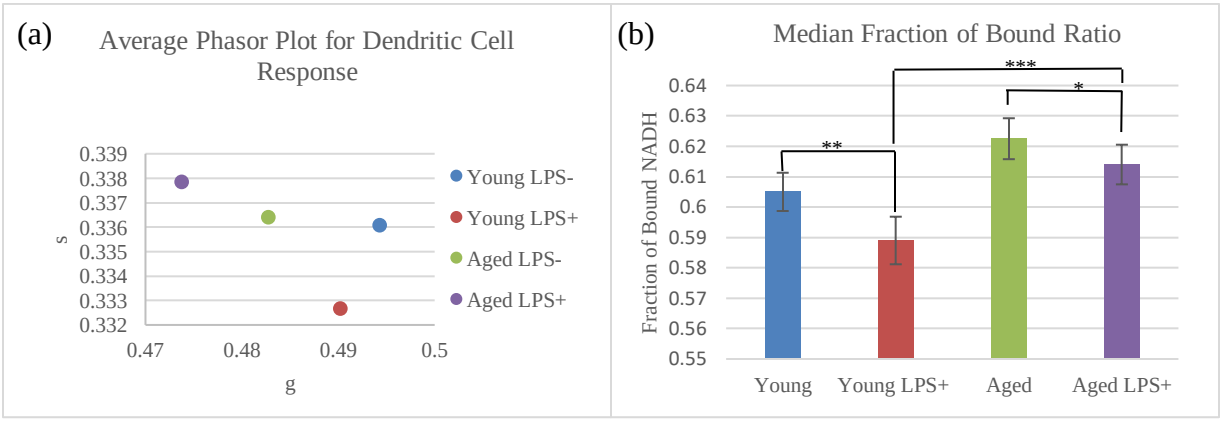

Figure 12: Dendritic Cell FLIM results. (a) Mean g and s values for each condition across all experiments plotted. (b) Median fraction of bound NADH in Young cells (n=337), Young LPS+ cells (n=193), Aged cells (n=217), Aged LPS+ cells (n=193). Wilcoxon signed-rank test yielded P-values. *P=0.051, **P=0.020, ***P=0.001. Standard Error plotted as error bars.

Fraction of bound ratios extracted through the analysis Globals for Images SimFCS of individual cells were compiled and categorized according to its corresponding subject and condition. Shapiro-Wilks Normality Test was ran for each set of data and yielded p-values all less than 0.05, therefore rejecting the hypothesis that the data sets are normally distributed. As such, non-parametric Wilcoxon Rank Sum test was used to perform statistical analysis.

4.4 Flow Cytometry Results

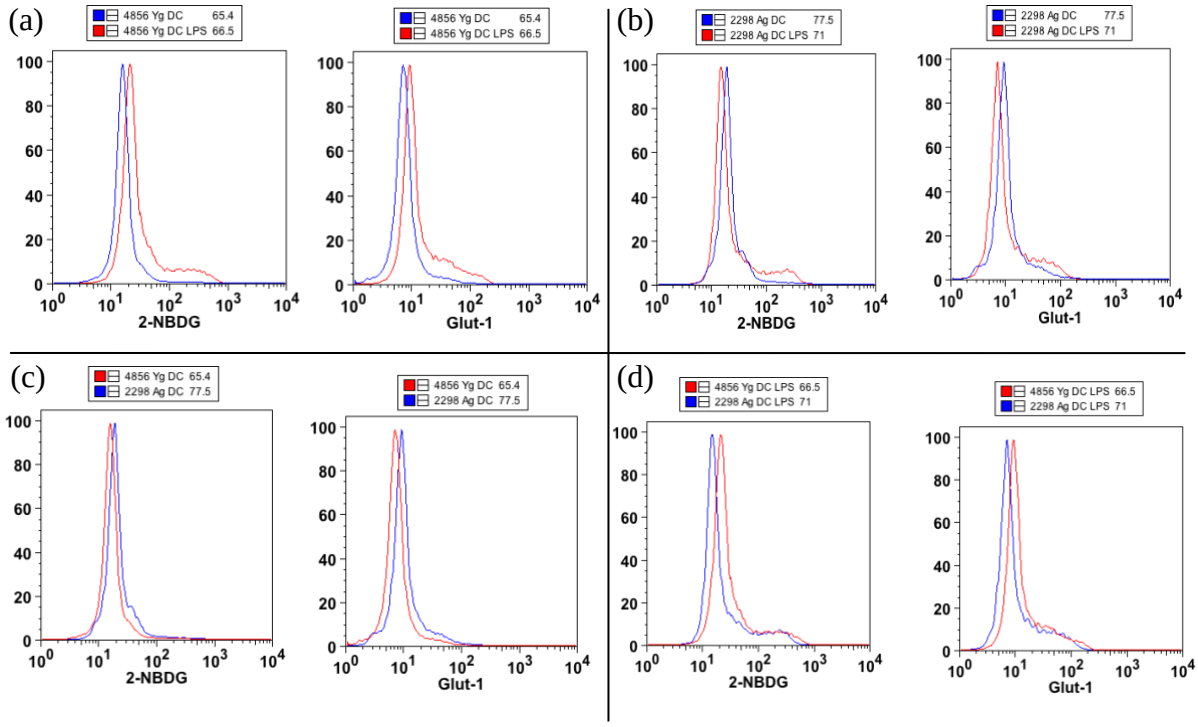

Figure 13: Flow cytometry histogram of a dendritic cell experiment. Each histogram plotted over 20,000 cells per condition. Cells were stained 2-NBDG and Glut 1 and read using FL-1 and FL-2 channel respectively. (a) Histogram of Young vs. Young LPS+ dendritic cells. (b) Histogram of Aged vs. Aged LPS+ dendritic cells. (c) Histogram of Young vs. Aged dendritic cells. (d) Histogram of Young LPS+ vs. Aged LPS+ dendritic cells

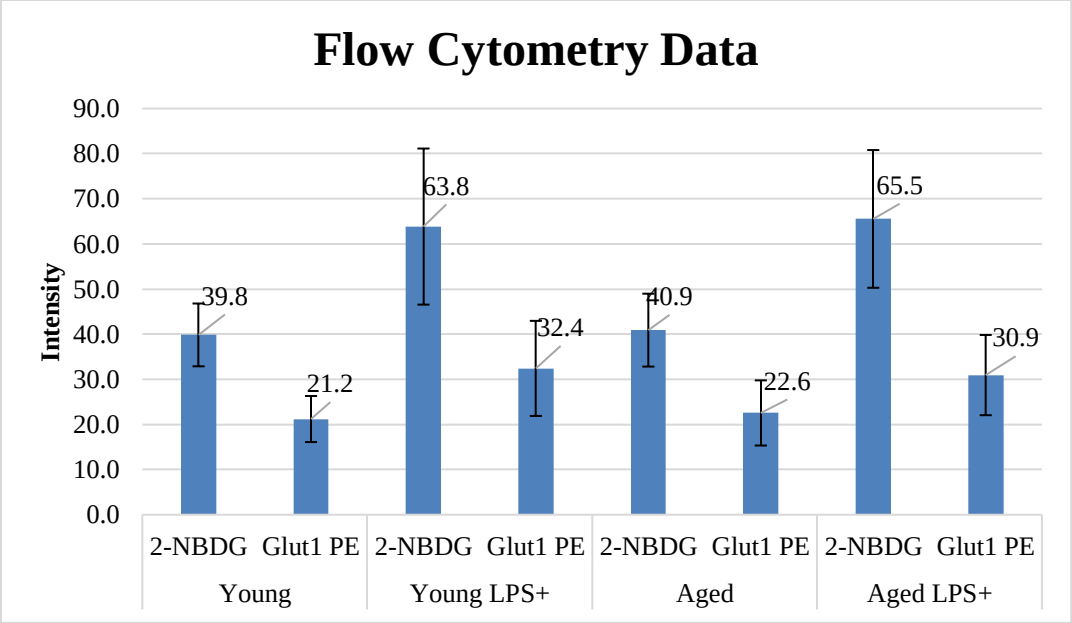

Figure 14: Dendritic cell flow cytometry results. Mean fluorescence intensity (MFI) was plotted across all conditions with standard error of the mean (SEM) as error bars.

The mean values from 2-NBDG FL-1 channel intensity and Glut1 PE FL-2 channel intensity were calculated for each subject's conditions. One standard error was applied to each condition as error bars in the figure above. There were no statistical significant differences in mean among all conditions (n=5, P-value>0.05), however we can observe the differences in mean. On average a 24 MFI increase in 2-NBDG expression and 11.2 MFI increase with Glut1 expression was observed in LPS activated cells in young subjects. With aged subjects, LPS activation resulted in an average of 24.6 and 8.3 MFI increase in 2-NBDG and Glut1 respectively. Across age groups, the increase in MFI is not as noticeable with only around one MFI difference between aged and young subjects with and without LPS activation.

CHAPTER 5: CONCLUSIONS

5.1 Statistical significance of data

Prefacing further data discussion, our data was not able to draw statistical significance between quiescent and activated cells with large variances in flow cytometry results across both age groups. FLIM results yielded significant differences between LPS activated cells and non-LPS activated cells (Figure 12), however, it is important to point out from Figure 11 we also observed large variances in single cell data. The minute differences between age group is expected as we are observing low grade inflammation as opposed to acute inflammation. We believe the variances within subjects was a result of cellular heterogeneity as our study performs single cell analysis of data. Cell heterogeneity is a phenomenon known for decades even from population of "seemingly identical cells"[83]. Moreover, some dendritic cells may be more activated than others with differing levels of cellular maturity. Thus, variations in the metabolic profile of DCs are thus expected. The variances between experiments can be attributed to human variability. Human subjects are notoriously hard to control, with differences in sex, race, genetics, diet, health conditioning, environment, and other elements all playing a factor in impacting the results. Nevertheless, we expect a baseline difference between the two age groups and use LPS as a positive control. The discussion below will examine the differences between subjects and LPS activation and attempt to interpret the findings based on the mean across all experiments.

5.2 Flow Cytometry Results

Despite not passing statistical significance, flow cytometry results yielded a large difference in mean between activated and quiescent cells. In one experiment, LPS activated DC displayed a 2.4-fold increase in MFI in 2-NBDG and 2.1-fold MFI increase Glut1signal.This supports our conjecture that LPS activated dendritic cells will undergo a drastic metabolic shift to meet the biosynthesis and bioenergetics needs of activated dendritic cells. These dendritic cells need a large amount of glucose to sustain the morphological changes, chemotaxis, and increased cytokine expression during DC activation[11]. However, there were no noticeable differences in glucose uptake between aged and young subjects (P-value>0.05, Figure 14). The result thus does not support our hypothesis that aging shift DCs towards higher glycolytic uptake due to more dendritic cell activation resulting from "inflammaging". Thus, in conjunction with FLIM results, we can more confidently infer that aging do not display Warburg effect on dendritic cell metabolism.

5.3 FLIM Results and Discussion

Previous studies in phasor FLIM analysis of free/bound NADH have established FLIM as a reliable tool in analyzing metabolic changes with cell. Mainly with more bound NADH the cell takes more of a OXPHOS dominant pathway and vice versa, with more free NADH, the cells take more of a glycolytic pathway[18,19,78,101]. With the further validation of our device through monitoring HeLa cell's response to 2-DG as control (Figure 10), we believe our phasor FLIM results to be accurate. The median fraction of bound NADH observed in LPS activated cells showed a statistically significant shift towards more free NADH in both young and aged subjects

(Figure 12). This result is consistent to previously published studies in murine models where cells take more of a glycolytic pathway once activated[13]. Further, the phasor FLIM results complement our flow cytometry results of which the LPS activated cells have taken up more glucose. As such, our data thus support the notion that to satisfy the inflammatory bioenergetics needs of the cells, DCs upregulates the aerobic glycolysis pathways (Figure 12, Figure 14).

As for metabolism comparing aged and young subjects, aging DCs displayed higher median fractional of bound NADH than young DCs. Following the logic that higher fractional bound NADH is indicative of a OXPHOS dominant pathway, the results are contrary to our proposed hypothesis that aging cells would take more of a glycolytic pathway. Aged LPS+ dendritic cells in fact showed much higher fraction of bound NADH compared to young LPS activated DCs (Figure 12, P-Value=0.001). Our hypothesis was based off the theory of "inflammaging", where aging subjects experience chronic inflammation and thus should have a more activated population of dendritic cells[2,102]. These activated dendritic cells would thus shift towards using Warburg metabolism resulting in a more glycolytic metabolic profile[11].

Nevertheless, the shift towards higher fraction of bounded NADH in aging, especially in LPS activated cells, seems significant and we'll attempt to conject the cause. This shift towards of higher fractional bound NADH may be a result of metabolic dysfunction, which is a hallmark of aging[103]. Conley *et al.* showed that elderly subjects' mitochondria displayed 50% lower oxidative capacity per volume of mitochondria[104]. It is thus conceivable that, to compensate, cells in elderly subjects upregulate OXPHOS activity to maintain the ATP output needed for cellular activity. The skew towards more fractional bound of NADH is more likely, however, due to the decreased overall levels of NAD with aging [105–110]. This decline of NAD was observed in both elderly mouse and human and is likely caused by the increased levels of CD38 and decreased activity of SIRT3 with aging[110]. CD38 is one of the main NADases that degrade NAD and is regulated by SIRT3. The decreased levels of NAD will thus bias the result into higher fractional amount of bound NADH compared to free since the total amount of NAD decreases. Decreased availability of NAD^+, and thus its reduced form NADH, will drive enzyme kinematics towards higher ratio of bound NADH as there are less substrates for the enzymes to bind to[18]. Therefore, it is possible that the effect of decreased levels of NAD in aging DCs was more significant than the effect of aging DCs shifting towards aerobic glycolysis due to low grade inflammation.

5.4 Concluding Remarks

Monocyte derived dendritic cells during inflammation have unique features and are known to produce large amounts of cytokines to regulate immune homeostasis[111,112]. These cytokines can be both pro-inflammatory (TNF-α, IL-6, IL-12) or anti-inflammatory (IL-10). During this state, DCs are referred to as "activated" and are capable of traveling to the lymph node to prime T-cells. Aging is often characterized by a low grade chronic inflammation that occurs in elderly subjects. Because of dendritic cells role in controlling inflammation, this study attempts to see if dendritic cells play a part in regulating this age related chronic inflammation by studying the metabolic changes in human DCs. In murine models, activated dendritic cells shifts towards a more glycolysis dominant pathway for energy production. We thus hypothesized that aging DCs would be more activated than young DCs due to this chronic inflammation and thus display a more glycolytic metabolic profile than young DCs.

The result of this study concludes that there are no statistically significant differences between dendritic cell metabolism between quiescent young and aged cells. The role of DC metabolic profile, thus, does not seem to play a large part in the deteriorating dendritic cell functions, "inflammaging," or immunosenescence. This is not to say that dendritic cells functionalities or mitochondria are not impacted by aging. As previously mentioned, other signaling pathways such as reduced phosphorylation of AKT in elderly, increased IFN regulatory factor 3, and increased NF-κB were observed in aged DCs[9,10]. These pathway changes in DCs are linked to aberrant DC cell behaviors and increased levels of pro-inflammatory cytokines in the elderly[102]. Other studies have shown that mitochondria volume and oxidative capacity decreases with age[104]. Our result thus joins a growing trend of data rejecting the notion that age related mitochondrial dysfunctions "are severe enough to cause the other degenerative phenotypes of aging" despite mitochondria often being implicated due to its ROS generation capability and degradation with age[113]. Further, while not significant, our data provides interesting trends that aging have increasing fractional of bound NADH compared to young subjects in both quiescent and activated samples. This hints that there are metabolic shifts with age, however, the etiology still needs to be further studied. Overall, this study provides a first look at the metabolic profiles of young and aged DCs in human subjects. The study is thus novel in that regard and hopes to open further interests in understanding metabolic changes with age.

5.5 Limitation of the Study

Due to time, budget, and donor availability constraints, only 7 experiments comparing aged and young subjects were performed. A more robust study with a human subject number closer to ~400 will yield a 95% confidence level in a population study[114]. With a larger sample size, statistical analysis should be able to provide more significant results with the data trends we are seeing. Moreover, the study was also limited by the variability introduce by the subject's race, sex, diet and other factors. Controlling these factors could potentially provide more consistent results but less representative of the human population. As for dendritic cells, while monocyte derived dendritic cells are great for *in vitro* studies, we do not know how they behave *in vivo*[115].There is also a wide subset of DCs that have heterogeneous functions, and this study only studies one of them[116]. For FLIM, there will be inevitable human bias and variability during image analysis. Since cells are selected and masked manually, there will be errors and prejudice in the selection and drawing the masks on the cells of fluorescent images. Lastly, for flow cytometry, the markers used for quantifying cellular respiration does not reveal the downstream pathway DCs take for glucose metabolism, mainly aerobic glycolysis or OXPHOS.

5.6 Future Work

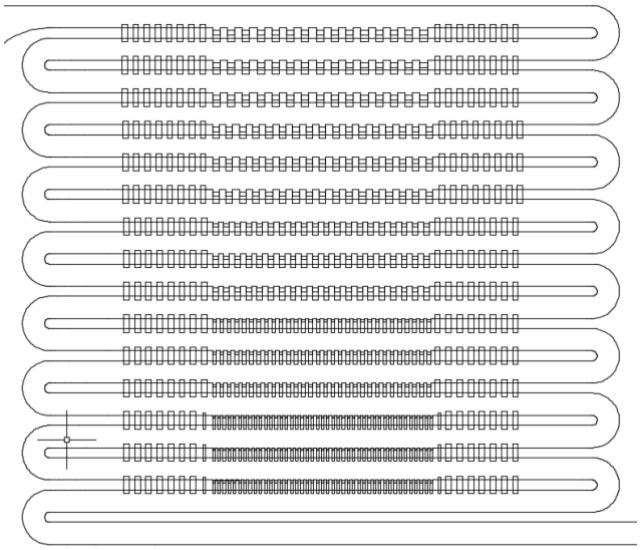

Figure 15: High throughput, variable trap size microfluidic design.

There are many research and techniques that could be further improved as detailed by the limitation of the study. First and foremost, increasing the amount of subject to allow a more robust study should be performed. This should allow our data to yield more significant results and provide a more accurate overview of the effect of aging on dendritic cell metabolism. *In vivo* intravital study of dendritic cells using a 2-Photon laser is possible on mice, however, not appropriate for human subjects[117,118] .Therefore, a more appropriate method would be to use e*x vivo* methods of extracting DCs to provide a more physiologically relevant model of DC behavior in human subjects[119,120]. For more mitochondrial assessment of DCs, analysis on the genetic and protein expression related to mitochondria functions such as succinate dehydrogenase, cytochrome c, and other subunits of electron transport chain complexes can be a useful method to monitor mitochondrial behavior. For example, Abcam offers an antibody kit (ab110413) that allows users to monitor 5 OXPHOS complexes. Other complimentary metabolic tests such as SeaHorse XF (Agilent) glycolysis stress test can further supplement the results. Adding these tests will provide more comprehensive and accurate view on cellular metabolism.

As for FLIM, more accurate image processing techniques to select and analyze cells should be developed. For exampling, using intensity separation techniques such as Arce *et al.*'s can be a useful automated, bias free tool to produce cell masks for analysis[121]. Machine learning algorithms with appropriate trained data sets could further increase the accuracy and separation of DCs for image analysis. These implementations not only increase the accuracy of the results but substantially reduce the image analysis time.

Lastly, our microfluidic platform for single cell trap can be further improved to increased throughput and efficiency (Figure 15). A variable cell trap design can be beneficial in trapping heterogeneous single DCs as they seem to vary by size with maturity levels [92]. Increasing the number of traps and further optimizing the flow to increase yield will be a logical improvement. Figure 15 shows an example of how cell trap can be varied while increasing the amount of cell traps. Testing other methodologies such as DiCarlo method and single cell droplets can also be viable approaches[21,88].

CHAPTER 6: REFERENCES

1. Liochev, S. Which Is the Most Significant Cause of Aging? *Antioxidants* (2015). doi:10.3390/antiox4040793
2. Franceschi, C. & Campisi, J. Chronic inflammation (Inflammaging) and its potential contribution to age-associated diseases. *Journals of Gerontology - Series A Biological Sciences and Medical Sciences* **69,** S4–S9 (2014).
3. Balistreri, C. R. Anti-Inflamm-Ageing and/or Anti-Age-Related Disease Emerging Treatments: A Historical Alchemy or Revolutionary Effective Procedures? *Mediators of Inflammation* (2018). doi:10.1155/2018/3705389
4. North, B. J. & Sinclair, D. A. The intersection between aging and cardiovascular disease. *Circulation Research* (2012). doi:10.1161/CIRCRESAHA.111.246876
5. FRANCESCHI, C. *et al.* Inflamm-aging: An Evolutionary Perspective on Immunosenescence. *Ann. N. Y. Acad. Sci.* (2006). doi:10.1111/j.1749-6632.2000.tb06651.x
6. Gupta, S. & Agrawal, A. Inflammation & autoimmunity in human ageing: Dendritic cells take a center stage. *Indian Journal of Medical Research* (2013).
7. Dall'Olio, F. *et al.* N-glycomic biomarkers of biological aging and longevity: A link with inflammaging. *Ageing Research Reviews* (2013). doi:10.1016/j.arr.2012.02.002
8. Agrawal, A., Agrawal, S. & Gupta, S. Role of dendritic cells in inflammation and loss of tolerance in the elderly. *Frontiers in Immunology* (2017). doi:10.3389/fimmu.2017.00896
9. Agrawal, A. Altered expression of NFkappaB in ex vivo differentiated dendritic cells from the aged subjects: implications in immunotherapy. *Methods Mol. Biol.* (2010). doi:10.1007/978-1-60761-063-2_12
10. Agrawal, A. *et al.* Altered Innate Immune Functioning of Dendritic Cells in Elderly Humans: A Role of Phosphoinositide 3-Kinase-Signaling Pathway. *J. Immunol.* (2007). doi:10.4049/jimmunol.178.11.6912
11. Pearce, E. J. & Everts, B. Dendritic cell metabolism. *Nat Rev Immunol* (2015). doi:10.1038/nri3771
12. Riol-Blanco, L. *et al.* The Chemokine Receptor CCR7 Activates in Dendritic Cells Two Signaling Modules That Independently Regulate Chemotaxis and Migratory Speed. *J. Immunol.* (2005). doi:10.4049/jimmunol.174.7.4070
13. Everts, B. *et al.* Commitment to glycolysis sustains survival of NO-producing inflammatory dendritic cells. *Blood* (2012). doi:10.1182/blood-2012-03-419747
14. Krawczyk, C. M. *et al.* Toll-like receptor-induced changes in glycolytic metabolism regulate dendritic cell activation. *Blood* **115,** 4742–4749 (2010).
15. O'Neill, L. A. J. & Pearce, E. J. Immunometabolism governs dendritic cell and macrophage function. *J. Exp. Med.* (2016). doi:10.1084/jem.20151570
16. Lakowicz, J. R., Szmacinski, H., Nowaczyk, K. & Johnson, M. L. Fluorescence lifetime imaging of free and protein-bound NADH. *Proc. Natl. Acad. Sci.* (1992). doi:10.1073/pnas.89.4.1271
17. Stringari, C. *et al.* Metabolic trajectory of cellular differentiation in small intestine by Phasor Fluorescence Lifetime Microscopy of NADH. *Sci. Rep.* (2012). doi:10.1038/srep00568
18. Cinco, R., Digman, M. A., Gratton, E. & Luderer, U. Spatial Characterization of

Bioenergetics and Metabolism of Primordial to Preovulatory Follicles in Whole Ex Vivo Murine Ovary. *Biol. Reprod.* (2016). doi:10.1095/biolreprod.116.142141
19. Lee, D.-H., Li, X., Ma, N., Digman, M. A. & Lee, A. P. Rapid and label-free identification of single leukemia cells from blood in a high-density microfluidic trapping array by fluorescence lifetime imaging microscopy. *Lab Chip* (2018). doi:10.1039/C7LC01301A
20. Li, X., Tao, Y., Lee, D.-H., Wickramasinghe, H. K. & Lee, A. P. In situ mRNA isolation from a microfluidic single-cell array using an external AFM nanoprobe. *Lab Chip* (2017). doi:10.1039/C7LC00133A
21. Carlo, D. Di, Wu, L. Y. & Lee, L. P. Dynamic single cell culture array. *Lab Chip* (2006). doi:10.1039/b605937f
22. Gerlinger, M. *et al.* Intratumor Heterogeneity and Branched Evolution Revealed by Multiregion Sequencing. *N. Engl. J. Med.* (2012). doi:10.1056/NEJMoa1113205
23. Lutz, W., Sanderson, W. & Scherbov, S. The coming acceleration of global population ageing. *Nature* (2008). doi:10.1038/nature06516
24. Weinstein, J. R. & Anderson, S. The Aging Kidney: Physiological Changes. *Advances in Chronic Kidney Disease* (2010). doi:10.1053/j.ackd.2010.05.002
25. Wyss-Coray, T. Ageing, neurodegeneration and brain rejuvenation. *Nature* (2016). doi:10.1038/nature20411
26. Aw, D., Silva, A. B. & Palmer, D. B. Immunosenescence: Emerging challenges for an ageing population. *Immunology* (2007). doi:10.1111/j.1365-2567.2007.02555.x
27. Campisi, J. Aging, Cellular Senescence, and Cancer. *Annu. Rev. Physiol.* (2013). doi:10.1146/annurev-physiol-030212-183653
28. Solana, R., Pawelec, G. & Tarazona, R. Aging and Innate Immunity. *Immunity* (2006). doi:10.1016/j.immuni.2006.05.003
29. Malaquin, N., Martinez, A. & Rodier, F. Keeping the senescence secretome under control: Molecular reins on the senescence-associated secretory phenotype. *Experimental Gerontology* (2016). doi:10.1016/j.exger.2016.05.010
30. Fransen, F. *et al.* Aged gut microbiota contributes to systemical inflammaging after transfer to germ-free mice. *Front. Immunol.* (2017). doi:10.3389/fimmu.2017.01385
31. John-Schuster, G. *et al.* Inflammaging increases susceptibility to cigarette smoke-induced COPD. *Oncotarget* (2015). doi:10.18632/oncotarget.4027
32. Bonafe, M., Storci, G. & Franceschi, C. Inflamm-aging of the stem cell niche: Breast cancer as a paradigmatic example. *BIOESSAYS* (2012). doi:10.1002/bies.201100104
33. Gallenga, C. E., Parmeggiani, F., Costagliola, C., Sebastiani, A. & Gallenga, P. E. Inflammaging: Should this term be suitable for age related macular degeneration too? *Inflammation Research* (2014). doi:10.1007/s00011-013-0684-2
34. Zhuang, Y. & Lyga, J. Inflammaging in Skin and Other Tissues - The Roles of Complement System and Macrophage. *Inflamm. Allergy-Drug Targets* (2014). doi:10.2174/1871528113666140522112003
35. Chen, M. & Xu, H. Parainflammation, chronic inflammation, and age-related macular degeneration. *J. Leukoc. Biol.* (2015). doi:10.1189/jlb.3RI0615-239R
36. Lencel, P. & Magne, D. Inflammaging: The driving force in osteoporosis? *Med. Hypotheses* (2011). doi:10.1016/j.mehy.2010.09.023
37. Perry, V. H. The influence of systemic inflammation on inflammation in the brain: Implications for chronic neurodegenerative disease. *Brain, Behavior, and Immunity* (2004). doi:10.1016/j.bbi.2004.01.004

38. Holmes, C. Systemic infection, interleukin 1beta, and cognitive decline in Alzheimer's disease. *J. Neurol. Neurosurg. Psychiatry* (2003). doi:10.1136/jnnp.74.6.788
39. Chinta, S. J. *et al.* Environmental stress, ageing and glial cell senescence: A novel mechanistic link to parkinson's disease? *J. Intern. Med.* (2013). doi:10.1111/joim.12029
40. Taniguchi, N., Kawakami, Y., Maruyama, I. & Lotz, M. HMGB proteins and arthritis. *Human Cell* (2018). doi:10.1007/s13577-017-0182-x
41. Wilson, D., Jackson, T., Sapey, E. & Lord, J. M. Frailty and sarcopenia: The potential role of an aged immune system. *Ageing Research Reviews* (2017). doi:10.1016/j.arr.2017.01.006
42. Baylis, D., Bartlett, D. B., Patel, H. P. & Roberts, H. C. Understanding how we age: insights into inflammaging. *Longev. Heal.* (2013). doi:10.1186/2046-2395-2-8
43. Schaap, L. A., Pluijm, S. M. F., Deeg, D. J. H. & Visser, M. Inflammatory Markers and Loss of Muscle Mass (Sarcopenia) and Strength. *Am. J. Med.* (2006). doi:10.1016/j.amjmed.2005.10.049
44. Morgan, S. A. *et al.* 11β-Hydroxysteroid Dehydrogenase Type 1 Regulates Glucocorticoid-Induced Insulin Resistance in Skeletal Muscle. *Diabetes* (2009). doi:10.2337/db09-0525
45. Giunta, B. *et al.* Inflammaging as a prodrome to Alzheimer's disease. *Journal of Neuroinflammation* (2008). doi:10.1186/1742-2094-5-51
46. Ishii, S. *et al.* C-reactive protein, bone strength, and nine-year fracture risk: data from the Study of Women's Health Across the Nation (SWAN). *J. Bone Miner. Res.* (2013). doi:10.1002/jbmr.1915
47. Agrawal, A., Agrawal, S. & Gupta, S. Dendritic cells in human aging. *Exp Gerontol* (2007). doi:10.1016/j.exger.2006.11.007
48. Naik, S. H. *et al.* Development of plasmacytoid and conventional dendritic cell subtypes from single precursor cells derived in vitro and in vivo. *Nat. Immunol.* (2007). doi:10.1038/ni1522
49. Hemmi, H. & Akira, S. TLR signalling and the function of dendritic cells. *Chem. Immunol. Allergy* (2005). doi:10.1159/000086657
50. Iwasaki, A. & Medzhitov, R. Toll-like receptor control of the adaptive immune responses. *Nature Immunology* (2004). doi:10.1038/ni1112
51. Schnare, M. *et al.* Toll-like receptors control activation of adaptive immune responses. *Nat Immunol* (2001). doi:10.1038/ni712
52. Geissmann, F. *et al.* Development of monocytes, macrophages, and dendritic cells. *Science* (2010). doi:10.1126/science.1178331
53. León, B., López-Bravo, M. & Ardavín, C. Monocyte-derived dendritic cells. *Seminars in Immunology* (2005). doi:10.1016/j.smim.2005.05.013
54. Banchereau, J. & Palucka, A. K. Dendritic cells as therapeutic vaccines against cancer. *Nature Reviews Immunology* (2005). doi:10.1038/nri1592
55. Della Bella, S. *et al.* Peripheral blood dendritic cells and monocytes are differently regulated in the elderly. *Clin. Immunol.* (2007). doi:10.1016/j.clim.2006.09.012
56. Shodell, M. & Siegal, F. P. Circulating, interferon-producing plasmacytoid dendritic cells decline during human ageing. *Scand. J. Immunol.* (2002). doi:10.1046/j.1365-3083.2002.01148.x
57. Steger, M. M., Maczek, C. & Grubeck-Loebenstein, B. Morphologically and functionally intact dendritic cells can be derived from the peripheral blood of aged individuals. *Clin.*

Exp. Immunol. (1996). doi:10.1046/j.1365-2249.1996.d01-790.x
58. Lung, T. L., Saurwein-Teissl, M., Parson, W., Schönitzer, D. & Grubeck-Loebenstein, B. Unimpaired dendritic cells can be derived from monocytes in old age and can mobilize residual function in senescent T cells. *Vaccine* (2000). doi:10.1016/S0264-410X(99)00494-6
59. Wong, C. & Goldstein, D. R. Impact of aging on antigen presentation cell function of dendritic cells. *Current Opinion in Immunology* (2013). doi:10.1016/j.coi.2013.05.016
60. Linton, P. J. & Dorshkind, K. Age-related changes in lymphocyte development and function. *Nature Immunology* (2004). doi:10.1038/ni1033
61. Pereira, L. F., Duarte de Souza, A. P., Borges, T. J. & Bonorino, C. Impaired in vivo CD4+ T cell expansion and differentiation in aged mice is not solely due to T cell defects: Decreased stimulation by aged dendritic cells. *Mech. Ageing Dev.* (2011). doi:10.1016/j.mad.2011.03.005
62. Kristiansen, O. P. & Mandrup-Poulsen, T. Interleukin-6 and Diabetes. *Diabetes* (2005). doi:10.2337/diabetes.54.suppl_2.S114
63. Nishimoto, N. Interleukin-6 in rheumatoid arthritis. *Current Opinion in Rheumatology* (2006). doi:10.1097/01.bor.0000218949.19860.d1
64. Edwards, C. J. & Williams, E. The role of interleukin-6 in rheumatoid arthritis-associated osteoporosis. *Osteoporosis International* (2010). doi:10.1007/s00198-010-1192-7
65. Athilingam, P. *et al.* Elevated levels of interleukin 6 and C-reactive protein associated with cognitive impairment in heart failure. *Congest. Heart Fail.* (2013). doi:10.1111/chf.12007
66. Huber, S. A., Sakkinen, P., Conze, D., Hardin, N. & Tracy, R. Interleukin-6 exacerbates early atherosclerosis in mice. *Arterioscler. Thromb. Vasc. Biol.* (1999). doi:10.1161/01.ATV.19.10.2364
67. Gatenby, R. A. & Gillies, R. J. Why do cancers have high aerobic glycolysis? *Nature Reviews Cancer* (2004). doi:10.1038/nrc1478
68. Heiden, M. G. Vander, Cantley, L. C. & Thompson, C. B. Understanding the warburg effect: The metabolic requirements of cell proliferation. *Science* (2009). doi:10.1126/science.1160809
69. Deberardinis, R. J. & Thompson, C. B. Cellular metabolism and disease: What do metabolic outliers teach us? *Cell* (2012). doi:10.1016/j.cell.2012.02.032
70. Heikal, A. A. Intracellular coenzymes as natural biomarkers for metabolic activities and mitochondrial anomalies. *Biomark. Med.* (2010). doi:10.2217/bmm.10.1
71. Medbo, J. I. & Tabata, I. Relative importance of aerobic and anaerobic energy release during short-lasting exhausting bicycle exercise. *J. Appl. Physiol.* (1989). doi:10.1152/jappl.1989.67.5.1881
72. Liberti, M. V. & Locasale, J. W. The Warburg Effect: How Does it Benefit Cancer Cells? *Trends in Biochemical Sciences* (2016). doi:10.1016/j.tibs.2015.12.001
73. Digman, M. A., Caiolfa, V. R., Zamai, M. & Gratton, E. The phasor approach to fluorescence lifetime imaging analysis. *Biophys. J.* **94,** (2008).
74. Van Munster, E. B. & Gadella, T. W. J. Fluorescence Lifetime Imaging Microscopy (FLIM). *Adv. Biochem. Eng. Biotechnol.* (2005). doi:10.1007/b102213
75. Stringari, C. *et al.* Multicolor two-photon imaging of endogenous fluorophores in living tissues by wavelength mixing. *Sci. Rep.* (2017). doi:10.1038/s41598-017-03359-8
76. Kasischke, K. A., Vishwasrao, H. D., Fisher, P. J., Zipfel, W. R. & Webb, W. W. Neural

activity triggers neuronal oxidative metabolism followed by astrocytic glycolysis. *Science (80-.).* (2004). doi:10.1126/science.1096485
77. Uchugonova, A. & König, K. Two-photon autofluorescence and second-harmonic imaging of adult stem cells. *J. Biomed. Opt.* (2008). doi:10.1117/1.3002370
78. Stringari, C. *et al.* Phasor approach to fluorescence lifetime microscopy distinguishes different metabolic states of germ cells in a live tissue. *Proc. Natl. Acad. Sci.* (2011). doi:10.1073/pnas.1108161108
79. Quinn, K. P. *et al.* Quantitative metabolic imaging using endogenous fluorescence to detect stem cell differentiation. *Sci. Rep.* (2013). doi:10.1038/srep03432
80. Dunn, D. A. & Feygin, I. Challenges and solutions to ultra-high-throughput screening assay miniaturization: Submicroliter fluid handling. *Drug Discovery Today* (2000). doi:10.1016/S1359-6446(00)80089-6
81. Squires, T. M. & Quake, S. R. Microfluidics: Fluid physics at the nanoliter scale. *Rev. Mod. Phys.* (2005). doi:10.1103/RevModPhys.77.977
82. Kochhar, J. S., Chan, S. Y., Ong, P. S., Lee, W. G. & Kang, L. *Microfluidic Devices for Biomedical Applications*. *Microfluidic Devices for Biomedical Applications* (2013). doi:10.1533/9780857097040.2.231
83. Altschuler, S. J. & Wu, L. F. Cellular Heterogeneity: Do Differences Make a Difference? *Cell* (2010). doi:10.1016/j.cell.2010.04.033
84. Tan, W.-H. & Takeuchi, S. A trap-and-release integrated microfluidic system for dynamic microarray applications. *Proc. Natl. Acad. Sci.* (2007). doi:10.1073/pnas.0606625104
85. Kobel, S., Valero, A., Latt, J., Renaud, P. & Lutolf, M. Optimization of microfluidic single cell trapping for long-term on-chip culture. *Lab Chip* (2010). doi:10.1039/b918055a
86. Chung, J., Kim, Y. J. & Yoon, E. Highly-efficient single-cell capture in microfluidic array chips using differential hydrodynamic guiding structures. *Appl. Phys. Lett.* (2011). doi:10.1063/1.3565236
87. Chen, Y. C. *et al.* Single-cell migration chip for chemotaxis-based microfluidic selection of heterogeneous cell populations. *Sci. Rep.* (2015). doi:10.1038/srep09980
88. Wen, N. *et al.* Development of droplet microfluidics enabling high-throughput single-cell analysis. *Molecules* (2016). doi:10.3390/molecules21070881
89. Brouzes, E. *et al.* Droplet microfluidic technology for single-cell high-throughput screening. *Proc. Natl. Acad. Sci.* (2009). doi:10.1073/pnas.0903542106
90. Mazutis, L. *et al.* Single-cell analysis and sorting using droplet-based microfluidics. *Nat. Protoc.* (2013). doi:10.1038/nprot.2013.046
91. Yesilkoy, F. *et al.* Highly efficient and gentle trapping of single cells in large microfluidic arrays for time-lapse experiments. *Biomicrofluidics* (2016). doi:10.1063/1.4942457
92. Dumortier, H. *et al.* Antigen Presentation by an Immature Myeloid Dendritic Cell Line Does Not Cause CTL Deletion In Vivo, but Generates CD8+ Central Memory-Like T Cells That Can Be Rescued for Full Effector Function. *J. Immunol.* **175,** 855–863 (2005).
93. Zou, C., Wang, Y. & Shen, Z. 2-NBDG as a fluorescent indicator for direct glucose uptake measurement. *J. Biochem. Biophys. Methods* **64,** 207–215 (2005).
94. Teslaa, T. & Teitell, M. A. Techniques to monitor glycolysis. *Methods Enzymol.* (2014). doi:10.1016/B978-0-12-416618-9.00005-4
95. Chen, C., Pore, N., Behrooz, A., Ismail-Beigi, F. & Maity, A. Regulation of glut1 mRNA by hypoxia-inducible factor-1: Interaction between H-ras and hypoxia. *J. Biol. Chem.* (2001). doi:10.1074/jbc.M010144200

96. Cho, S. J., Moon, J. S., Lee, C. M., Choi, A. M. K. & Stout-Delgado, H. W. Glucose transporter 1-dependent glycolysis is increased during aging-related lung fibrosis, and phloretin inhibits lung fibrosis. *Am. J. Respir. Cell Mol. Biol.* (2017). doi:10.1165/rcmb.2016-0225OC
97. Choi, S. & Park, J.-K. Two-step photolithography to fabricate multilevel microchannels. *Biomicrofluidics* (2010). doi:10.1063/1.3517230
98. Murphy, M. P. How mitochondria produce reactive oxygen species. *Biochem. J.* (2009). doi:10.1042/BJ20081386
99. Ott, M., Gogvadze, V., Orrenius, S. & Zhivotovsky, B. Mitochondria, oxidative stress and cell death. *Apoptosis* (2007). doi:10.1007/s10495-007-0756-2
100. Mazur, M. T. & Williamson, J. R. Macrophage deformability and phagocytosis. *J. Cell Biol.* (1977).
101. Pate, K. T. *et al.* Wnt signaling directs a metabolic program of glycolysis and angiogenesis in colon cancer. *EMBO J.* (2014). doi:10.15252/embj.201488598
102. Agrawal, A., Agrawal, S. & Gupta, S. Role of Dendritic Cells in Aging. in *Handbook on Immunosenescence* (ed. Fulop T., Franceschi C., Hirokawa K., P. G.) 1–15 (Springer, Cham, 2018). doi:https://doi.org/10.1007/978-3-319-64597-1_25-1
103. López-Otín, C., Blasco, M. A., Partridge, L., Serrano, M. & Kroemer, G. The hallmarks of aging. *Cell* (2013). doi:10.1016/j.cell.2013.05.039
104. Conley, K. E., Jubrias, S. A. & Esselman, P. C. Oxidative capacity and ageing in human muscle. *J. Physiol.* (2000). doi:10.1111/j.1469-7793.2000.t01-1-00203.x
105. Zhu, X.-H., Lu, M., Lee, B.-Y., Ugurbil, K. & Chen, W. In vivo NAD assay reveals the intracellular NAD contents and redox state in healthy human brain and their age dependences. *Proc. Natl. Acad. Sci.* (2015). doi:10.1073/pnas.1417921112
106. Gomes, A. P. *et al.* Declining NAD+induces a pseudohypoxic state disrupting nuclear-mitochondrial communication during aging. *Cell* (2013). doi:10.1016/j.cell.2013.11.037
107. Braidy, N. *et al.* Age related changes in NAD+ metabolism oxidative stress and sirt1 activity in wistar rats. *PLoS One* (2011). doi:10.1371/journal.pone.0019194
108. Schultz, M. B. & Sinclair, D. A. Why NAD+ Declines during Aging: It's Destroyed. *Cell Metabolism* (2016). doi:10.1016/j.cmet.2016.05.022
109. Massudi, H. *et al.* Age-associated changes in oxidative stress and NAD+ metabolism in human tissue. *PLoS One* (2012). doi:10.1371/journal.pone.0042357
110. Camacho-Pereira, J. *et al.* CD38 Dictates Age-Related NAD Decline and Mitochondrial Dysfunction through an SIRT3-Dependent Mechanism. *Cell Metab.* (2016). doi:10.1016/j.cmet.2016.05.006
111. Plantinga, M. *et al.* Conventional and Monocyte-Derived CD11b+ Dendritic Cells Initiate and Maintain T Helper 2 Cell-Mediated Immunity to House Dust Mite Allergen. *Immunity* (2013). doi:10.1016/j.immuni.2012.10.016
112. Sprangers, S., Vries, T. J. D. & Everts, V. Monocyte Heterogeneity: Consequences for Monocyte-Derived Immune Cells. *Journal of Immunology Research* (2016). doi:10.1155/2016/1475435
113. Wang, Y. & Hekimi, S. Mitochondrial dysfunction and longevity in animals: Untangling the knot. *Science* (2015). doi:10.1126/science.aac4357
114. Kadam, P. & Bhalerao, S. Sample size calculation. *Int. J. Ayurveda Res.* (2010). doi:10.4103/0974-7788.59946
115. O'Neill, H. C. & Wilson, H. L. Limitations with in vitro production of dendritic cells

using cytokines. *J. Leukoc. Biol.* (2004). doi:10.1189/jlb.0903446
116. Segura, E. Review of Mouse and Human Dendritic Cell Subsets. in *Dendritic Cell Protocols* (2016). doi:10.1016/S0264-410X(02)00612-6
117. van Panhuys, N. Studying dendritic cell-T cell interactions under in vivo conditions. in *Methods in Molecular Biology* (2017). doi:10.1007/978-1-4939-6881-7_36
118. Kitano, M. *et al.* Imaging of the cross-presenting dendritic cell subsets in the skin-draining lymph node. *Proc. Natl. Acad. Sci.* (2016). doi:10.1073/pnas.1513607113
119. Araki, H. *et al.* Efficient ex vivo generation of dendritic cells from CD14+ blood monocytes in the presence of human serum albumin for use in clinical vaccine trials. *Br. J. Haematol.* (2001). doi:10.1046/j.1365-2141.2001.02973.x
120. Nair, S., Archer, G. E. & Tedder, T. F. *Isolation and generation of human dendritic cells. Current protocols in immunology / edited by John E. Coligan ... [et al.]* (2012). doi:10.1002/0471142735.im0732s99
121. Arce, S. H., Wu, P. H. & Tseng, Y. Fast and accurate automated cell boundary determination for fluorescence microscopy. *Sci. Rep.* (2013). doi:10.1038/srep02266